Stabilization of evanescent wave propagation operators

Andersson, Michael; Sjöberg, Daniel; Kristensson, Gerhard

2022

CODEN:LUTEDX/(TEAT-7274)/1-35/(2022)

Stabilization of evanescent wave propagation operators

Michael Andersson, Daniel Sjöberg and Gerhard Kristensson

Electromagnetic Theory
Department of Electrical and Information Technology
Lund University
Sweden

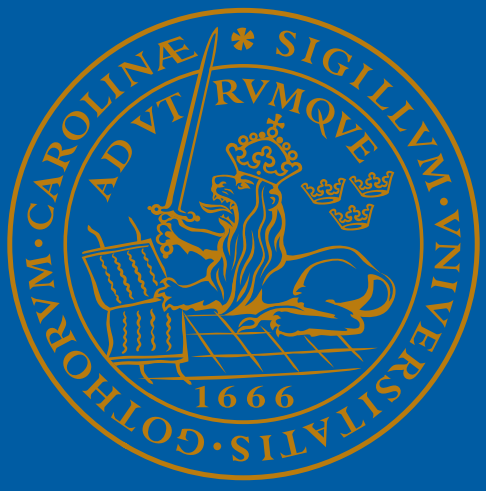

(TEAT-7274)/1-35/(2022): M. Andersson, Stabilization of evanescent wave propagation operators

Michael Andersson
michael.andersson@eit.lth.se

Department of Electrical and Information Technology
Electromagnetic Theory
Lund University
P.O. Box 118
SE-221 00 Lund
Sweden

Editor: Mats Gustafsson

Abstract

This paper presents a stabilized scheme that solves the wave propagation problem in a general bianisotropic, stratified medium. The method utilizes the concept of propagators, *i.e.*, the wave propagation operators that map the total tangential electric and magnetic fields from one plane in the slab to another. The scheme transforms the propagator approach into a scattering matrix form, where a spectral decomposition of the propagator enables separation of the exponentially growing and decaying terms in order to obtain a well-conditioned formulation. Multilayer structures can be handled in a stable manner using the dissipative property of the Redheffer star product for cascading scattering matrices. The reflection and transmission dyadics for a general bianisotropic medium with an isotropic half space on both sides of the slab are presented in a coordinate-independent dyadic notation, as well as the reflection dyadic for a bianisotropic slab with perfect electric conductor backing (PEC). Several numerical examples that illustrate the performance of the stabilized algorithm are presented.

1 Introduction

Structures that are layered in one coordinate direction, and possibly but not necessarily homogeneous in the remaining two, are common in nature as well as in microwave and optical devices. Such structures take their full description in three dimensions (3D), but their scattering properties are often considered in a one-dimensional (1D) setting, which reduces the complexity of the problem considerably. Methods reducing 3D problems to 1D are referred to as semi-analytical, and have been of great interest in the past, and are in fact still of considerable importance in practice, *e.g.*, in the design and optimization process of many types of structures with electromagnetic functionality [31]. The parameter space needed to be considered in the optimization process of an electromagnetic device is typically very large with many local minima [3], which in practice implies that initial simulations are commonly performed by the use of simplified methods like 1D approximations [5, 10, 38], and the move to full 3D modelling is, if even possible, only done for verification and tuning of the final design of the device.

Simplifications where the microstructure is replaced with a macroscopic description can be accomplished by the use of, *e.g.*, homogenization techniques [16, 23, 29, 32], that gives an effective medium approximation of the device. Alternatively, it is common to use equivalent-circuit techniques in order to approximate complex devices [11, 33, 34, 37]. Modeling approaches based on the standard transfer or scattering matrix methods for stratified systems are classical, and adapted versions of the methods to analyze behaviors of metasurface stacks have been recently reported in the literature [1, 17, 35].

This paper is focused on the propagator method, which is an approach adapted for solving 1D scattering problems of planar stratified structures, where the slabs in general can be arbitrary linear materials, *i.e.*, bianisotropic materials [9, 30]. The propagator technique can also be seen as a vector generalization of the transmission

(ABCD) matrix [25], or as a generalization of wave propagation through homogeneous media modeled as a transmission line [33]. The propagator method is in fact most closely related to the less known wave matrix formulation reported in [26].

The propagator method is for most purposes accurate, but the formulation is in fact inherently unstable, which is a well known common characteristics of other related transfer and scattering matrix approaches. Historically, there has been a desire to reformulate these methods in a numerically stable manner and several stabilized schemes have been developed in the past [6, 12, 13, 15, 19, 24, 36]. More recent works that call for well-conditioned formulations are reported in [4, 18]. Numerical problems with the propagator formalism were early pointed out in [36], that stabilized the reflection problem by use of a spectral recursive transformation method. Our paper introduces a reformulation of the propagator method [9, 30], that solves the reflection as well as the transmission problem, by changing the approach into a scattering matrix formulation, where the exponentially growing and decaying terms are separated, resulting in a well-conditioned formulation. Having a stable and robust scattering matrix formulation for each slab in a given multilayer stack, the total scattering matrix, *i.e.*, the composition of the individual scattering matrices, is then constructed by use of the Redheffer star product technique [27]. The dissipation property of the star product ensures the numerical stability of the algorithm for single as well as multilayer structures.

The stabilization of the propagator approach has been driven by the need of extending its applicability to accurately handling devices that support evanescent wave modes such as structures made up of complex materials that exhibit strong dispersion within the frequency band of interest, or multilayered periodic bandgap devices. The propagator can also be used in connection with frequency selective surfaces (FSS) [8], where evanescent wave modes are present. Recently [7] made a stability improvement due to the presence of higher order modes when considering the problem of multi-modal scattering and propagation through several closely spaced periodic grids. The methodology presented in this paper is a building block in handling similar higher order mode couplings through evanescent waves.

The present paper is organized as follows. The propagator method is revisited in Chapter 2, and the inherently unstable nature of the method is explained and illustrated by numerical examples in Chapter 3. The wave and scattering matrix forms are discussed in Chapter 4 in connection with the stable reformulation of the propagator method. The composition of a stack of slabs by the star product is revisited in Chapter 5. The numerical accuracy and stability of the new formulation are verified in Chapter 6. A summary with conclusions are given in Chapter 7, and an Appendix including basic equations and relations are included at the end of the paper.

2 Summary of the propagator method

This section summarizes the propagator method, which constitutes a systematic analysis that solves the wave propagation problem in a general bianisotropic layered

medium. A more detailed presentation of the propagator method is found in [9, 30], and references therein. The foundation of the method is the notion of the propagator, *i.e.*, the wave propagation operator that maps the total tangential electric and magnetic fields from one plane in the slab to another. This is in contrast to the more common approach of propagating the eigenmodes, *i.e.*, the forward and backward moving modes of the slab.

The reflection and transmission problem is treated in a concise way using a coordinate-free dyadic notation. The reflection and transmission dyadics for a medium enclosed with isotropic half spaces on both sides is presented as well as the reflection dyadic for a medium with perfect electric conductor (PEC) backing. The current on the metal backing of the latter case is also given.

The formulation presented in this chapter extends the earlier reported method for the treatment of an arbitrary background medium distinct from vacuum by introducing the concept of relative wave impedance operators in accordance with Appendix D.

2.1 The plane wave spectrum representation

For the purpose of studying wave propagation in layered media as illustrated in Figure 1, it is appropriate to decompose the electromagnetic field in a spectrum of plane waves by use of the Fourier transform in the lateral variables in accordance with Appendix A. We adopt the time convention $\mathrm{e}^{-\mathrm{i}\omega t}$, and provided all the generating sources are located in the isotropic half-space $z < z_0$, the incident, reflected, and transmitted fields are given by

$$\boldsymbol{E}^{\mathrm{i}}(\boldsymbol{r},\omega) = \frac{1}{4\pi^2}\iint_{-\infty}^{\infty}\left(\mathbf{I}_2 - \frac{\hat{\boldsymbol{z}}\boldsymbol{k}_{\mathrm{t}}}{k_{\mathrm{z}}}\right)\cdot\boldsymbol{F}^{+}(\boldsymbol{k}_{\mathrm{t}},z_1)\mathrm{e}^{\mathrm{i}\boldsymbol{k}_{\mathrm{t}}\cdot\boldsymbol{\rho}+\mathrm{i}k_{\mathrm{z}}(z-z_1)}\,\mathrm{d}k_{\mathrm{x}}\,\mathrm{d}k_{\mathrm{y}} \tag{2.1}$$

$$\boldsymbol{E}^{\mathrm{r}}(\boldsymbol{r},\omega) = \frac{1}{4\pi^2}\iint_{-\infty}^{\infty}\left(\mathbf{I}_2 + \frac{\hat{\boldsymbol{z}}\boldsymbol{k}_{\mathrm{t}}}{k_{\mathrm{z}}}\right)\cdot\mathbf{r}^{+}\cdot\boldsymbol{F}^{+}(\boldsymbol{k}_{\mathrm{t}},z_1)\mathrm{e}^{\mathrm{i}\boldsymbol{k}_{\mathrm{t}}\cdot\boldsymbol{\rho}-\mathrm{i}k_{\mathrm{z}}(z-z_1)}\,\mathrm{d}k_{\mathrm{x}}\,\mathrm{d}k_{\mathrm{y}} \tag{2.2}$$

$$\boldsymbol{E}^{\mathrm{t}}(\boldsymbol{r},\omega) = \frac{1}{4\pi^2}\iint_{-\infty}^{\infty}\left(\mathbf{I}_2 - \frac{\hat{\boldsymbol{z}}\boldsymbol{k}_{\mathrm{t}}}{k_{\mathrm{z}}}\right)\cdot\mathbf{t}^{+}\cdot\boldsymbol{F}^{+}(\boldsymbol{k}_{\mathrm{t}},z_1)\mathrm{e}^{\mathrm{i}\boldsymbol{k}_{\mathrm{t}}\cdot\boldsymbol{\rho}+\mathrm{i}k_{\mathrm{z}}(z-z_{N-1})}\,\mathrm{d}k_{\mathrm{x}}\,\mathrm{d}k_{\mathrm{y}} \tag{2.3}$$

Here, (2.1) is valid in the region $z_0 \leqslant z \leqslant z_1$, (2.2) in $z \leqslant z_1$, and (2.3) in $z \geqslant z_{N-1}$.

Furthermore, $\boldsymbol{F}^{+}(\boldsymbol{k}_{\mathrm{t}},z_1)$ is the Fourier component of the transverse, electric excitation at the interface $z = z_1$, and $\mathbf{r}^{+}$ and $\mathbf{t}^{+}$ denote the reflection and transmission dyadics for excitation from the left, see Section 2.5. Here, $\boldsymbol{\rho} = x\hat{\boldsymbol{x}} + y\hat{\boldsymbol{y}}$ is the transverse position vector, $\boldsymbol{k}_{\mathrm{t}} = k_{\mathrm{x}}\hat{\boldsymbol{x}} + k_{\mathrm{y}}\hat{\boldsymbol{y}}$ is the transverse wave vector, $\mathbf{I}_2 = \hat{\boldsymbol{x}}\hat{\boldsymbol{x}} + \hat{\boldsymbol{y}}\hat{\boldsymbol{y}}$ is the transverse identity dyadic, and $\hat{\boldsymbol{x}}$, $\hat{\boldsymbol{y}}$, and $\hat{\boldsymbol{z}}$ are the unit vectors in the x, y, and z coordinate directions. Finally, the longitudinal wave number k_{z} is given by (where $k_{\mathrm{t}} = |\boldsymbol{k}_{\mathrm{t}}|$ and k is the wavenumber in the isotropic material)

$$k_{\mathrm{z}} = \begin{cases} \sqrt{k^2 - k_{\mathrm{t}}^2} & k_{\mathrm{t}} < k \\ \mathrm{i}\sqrt{k_{\mathrm{t}}^2 - k^2} & k_{\mathrm{t}} > k \end{cases} \tag{2.4}$$

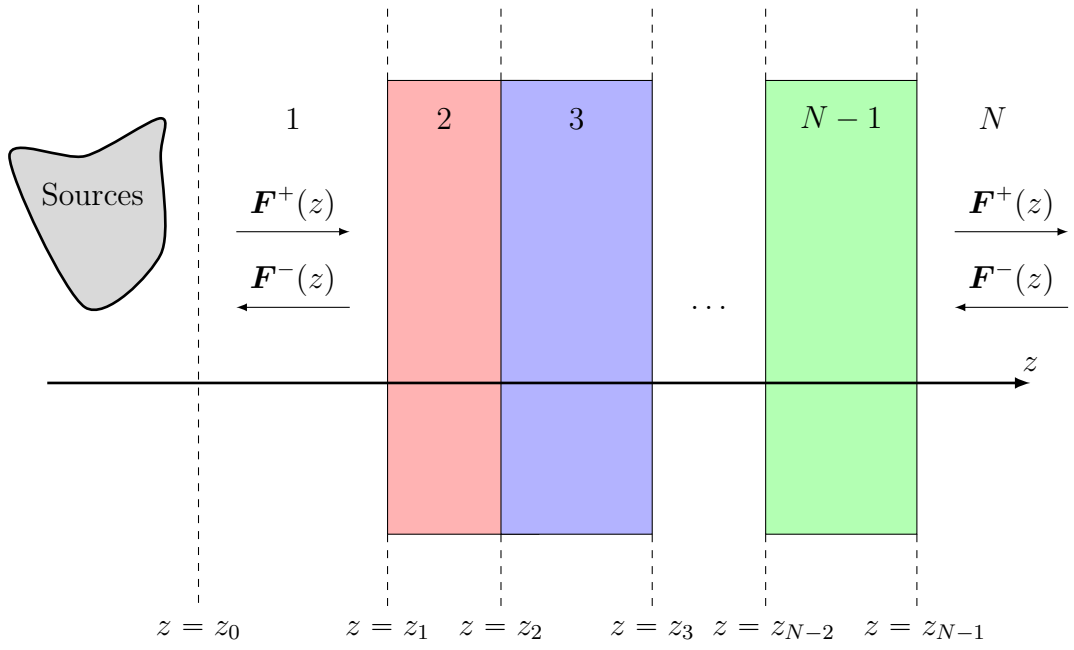

Figure 1: The source region $z < z_0 < z_1$ and symbolic representation of the left and right propagating split fields $\boldsymbol{F}^{\pm}$ in region 1 and N, outside the stratified region. The extent of the source region is limited by the plane $z = z_0$.

We assume the isotropic regions are lossless, hence the wavenumber k is real and positive. In general, the surrounding isotropic regions could have different material parameters, *i.e.*, we could have $k = k_{\mathrm{a}}$ in (2.1) and (2.2), whereas $k = k_{\mathrm{b}}$ in (2.3), where k_{a} and k_{b} are the wavenumbers for the different materials.

2.2 The fundamental equation

From now on, the tangential wave vector, $\boldsymbol{k}_{\mathrm{t}}$, is assumed being fixed but arbitrary. The Fourier components of the electric and magnetic fields can be uniquely decomposed in their tangential and normal components as

$$\begin{cases} \boldsymbol{E}(\boldsymbol{k}_{\mathrm{t}}, z) = \boldsymbol{E}_{\mathrm{t}}(\boldsymbol{k}_{\mathrm{t}}, z) + \hat{\boldsymbol{z}} E_{\mathrm{z}}(\boldsymbol{k}_{\mathrm{t}}, z) \\ \boldsymbol{H}(\boldsymbol{k}_{\mathrm{t}}, z) = \boldsymbol{H}_{\mathrm{t}}(\boldsymbol{k}_{\mathrm{t}}, z) + \hat{\boldsymbol{z}} H_{\mathrm{z}}(\boldsymbol{k}_{\mathrm{t}}, z) \end{cases} \tag{2.5}$$

Substituting the constitutive relations describing the material into the Maxwell equations (see Appendix B.1 and B.2 for further details) and eliminating the normal field components E_{z} and H_{z}, gives a system of ordinary differential equations (ODEs) in the tangential components of the electric and magnetic fields only. The fundamental equation for one-dimensional time-harmonic wave propagation becomes [9]

$$\frac{\mathrm{d}}{\mathrm{d}z} \begin{pmatrix} \boldsymbol{E}_{\mathrm{t}}(\boldsymbol{k}_{\mathrm{t}}, z) \\ \eta_0 \mathbf{J} \cdot \boldsymbol{H}_{\mathrm{t}}(\boldsymbol{k}_{\mathrm{t}}, z) \end{pmatrix} = \mathrm{i}k_0 \mathbf{M}(\boldsymbol{k}_{\mathrm{t}}, z) \cdot \begin{pmatrix} \boldsymbol{E}_{\mathrm{t}}(\boldsymbol{k}_{\mathrm{t}}, z) \\ \eta_0 \mathbf{J} \cdot \boldsymbol{H}_{\mathrm{t}}(\boldsymbol{k}_{\mathrm{t}}, z) \end{pmatrix} \tag{2.6}$$

where $\mathbf{J} = \hat{\boldsymbol{z}} \times \mathbf{I}_2$ is a rotation in the x-y-plane by $\pi/2$, and $\mathbf{M}(\boldsymbol{k}_\mathrm{t}, z)$ is a 4×4 complex-valued dyadic referred to as the fundamental dyadic.

Equation (2.6) is the general equation for wave propagation in linear, laterally homogeneous media. From the solution of this equation, can the longitudinal parts of the fields and flux densities be found [9].

2.3 Wave propagation operators

The propagator formalism makes use of the fact that the total tangential electric and magnetic fields are continuous across the interfaces in a planar stratified structure as illustrated in Figure 1. Thus, the propagator, *i.e.*, the wave propagation operator, maps the total tangential electric and magnetic fields at the front surface of the structure to the total tangential electric and magnetic fields at the rear surface of the structure.

2.3.1 Single layer

A formal solution to the fundamental equation (2.6) can be written [9]

$$\begin{pmatrix} \boldsymbol{E}_\mathrm{t}(\boldsymbol{k}_\mathrm{t}, z) \\ \eta_0 \mathbf{J} \cdot \boldsymbol{H}_\mathrm{t}(\boldsymbol{k}_\mathrm{t}, z) \end{pmatrix} = \mathbf{P}(\boldsymbol{k}_\mathrm{t}, z, z_1) \cdot \begin{pmatrix} \boldsymbol{E}_\mathrm{t}(\boldsymbol{k}_\mathrm{t}, z_1) \\ \eta_0 \mathbf{J} \cdot \boldsymbol{H}_\mathrm{t}(\boldsymbol{k}_\mathrm{t}, z_1) \end{pmatrix} \tag{2.7}$$

where the propagator $\mathbf{P}$ is a 4×4 complex-valued dyadic, mapping the tangential electric and magnetic fields from z_1 to z. For a homogeneous material, an explicit solution of (2.6) can be found, and in this case the propagator is (note that the order of the z-arguments in the propagator is important)

$$\mathbf{P}(\boldsymbol{k}_\mathrm{t}, z, z_1) = \mathrm{e}^{\mathrm{i}k_0(z-z_1)\mathbf{M}(\boldsymbol{k}_\mathrm{t})} \tag{2.8}$$

where the fundamental dyadic $\mathbf{M}$ contains all the wave propagation properties of the slab and the exponential function propagates the field from one position z_1 to another position z. Note that (2.7) is a transfer matrix form that relates the total tangential electric and magnetic fields between boundaries [26].

2.3.2 Several layers

Let z_j, $j = 1, \ldots, N-1$, be the locations of $N-1$ parallel interfaces, as depicted in Figure 1, and let $\mathbf{M}_j$, $j = 1, \ldots, N$, be the fundamental dyadics of the corresponding regions, respectively. It is assumed that all slabs are homogeneous and that the environmental regions $j = 1$ and $j = N$ are isotropic and homogeneous.

Since the tangential electric and magnetic fields are continuous at the boundaries, a cascade coupling technique can be applied. Using (2.8) repeatedly gives

$$\begin{pmatrix} \boldsymbol{E}_\mathrm{t}(\boldsymbol{k}_\mathrm{t}, z_{N-1}) \\ \eta_0 \mathbf{J} \cdot \boldsymbol{H}_\mathrm{t}(\boldsymbol{k}_\mathrm{t}, z_{N-1}) \end{pmatrix} = \mathbf{P}(z_{N-1}, z_1) \cdot \begin{pmatrix} \boldsymbol{E}_\mathrm{t}(\boldsymbol{k}_\mathrm{t}, z_1) \\ \eta_0 \mathbf{J} \cdot \boldsymbol{H}_\mathrm{t}(\boldsymbol{k}_\mathrm{t}, z_1) \end{pmatrix} \tag{2.9}$$

where the propagator for the layered bianisotropic structure is

$$\mathbf{P}(z_{N-1}, z_1) = \mathrm{e}^{\mathrm{i}k_0(z_{N-1}-z_{N-2})\mathbf{M}_{N-1}} \cdot \ldots \cdot \mathrm{e}^{\mathrm{i}k_0(z_3-z_2)\mathbf{M}_3} \cdot \mathrm{e}^{\mathrm{i}k_0(z_2-z_1)\mathbf{M}_2} \tag{2.10}$$

Hence, the propagator for a layered structure is given by the product of the propagators for each layer. Note that in general the dyadics do not commute, so the order of the products matter.

2.4 Wave splitting in simple medium

In order to efficiently organize the solution of the wave propagation problem, we introduce a wave splitting in the isotropic regions surrounding the stratified region. The wave splitting is a one-to-one transformation between the total tangential fields $\boldsymbol{E}_{\mathrm{t}}$ and $\eta_0 \mathbf{J} \cdot \boldsymbol{H}_{\mathrm{t}}$, respectively, and two new split fields $\boldsymbol{F}^{+}$ and $\boldsymbol{F}^{-}$, *i.e.*, forward and backward traveling fields, respectively.

This section extends the vacuum wave splitting reported in [9, 30] to any linear homogeneous and isotropic medium, which is relevant if the layered structure is being enclosed by an isotropic material distinct from vacuum.

By introducing the relative wave impedance operator $\mathbf{Z}_{\mathrm{r}}$ that relates the electric and magnetic fields propagating in the $\pm z$-direction through

$$\eta_0 \mathbf{J} \cdot \boldsymbol{H}_{\mathrm{t}}(\boldsymbol{k}_{\mathrm{t}}, z) = \mp \mathbf{Z}_{\mathrm{r}}^{-1}(\boldsymbol{k}_{\mathrm{t}}) \cdot \boldsymbol{E}_{\mathrm{t}}(\boldsymbol{k}_{\mathrm{t}}, z) \tag{2.11}$$

see Appendix D, the wave splitting in any isotropic, homogeneous medium, becomes

$$\begin{pmatrix} \boldsymbol{F}^{+}(\boldsymbol{k}_{\mathrm{t}}, z) \\ \boldsymbol{F}^{-}(\boldsymbol{k}_{\mathrm{t}}, z) \end{pmatrix} = \frac{1}{2} \begin{pmatrix} \mathbf{I}_2 & -\mathbf{Z}_{\mathrm{r}} \\ \mathbf{I}_2 & \mathbf{Z}_{\mathrm{r}} \end{pmatrix} \cdot \begin{pmatrix} \boldsymbol{E}_{\mathrm{t}}(\boldsymbol{k}_{\mathrm{t}}, z) \\ \eta_0 \mathbf{J} \cdot \boldsymbol{H}_{\mathrm{t}}(\boldsymbol{k}_{\mathrm{t}}, z) \end{pmatrix} \tag{2.12}$$

with inverse

$$\begin{pmatrix} \boldsymbol{E}_{\mathrm{t}}(\boldsymbol{k}_{\mathrm{t}}, z) \\ \eta_0 \mathbf{J} \cdot \boldsymbol{H}_{\mathrm{t}}(\boldsymbol{k}_{\mathrm{t}}, z) \end{pmatrix} = \begin{pmatrix} \mathbf{I}_2 & \mathbf{I}_2 \\ -\mathbf{Z}_{\mathrm{r}}^{-1} & \mathbf{Z}_{\mathrm{r}}^{-1} \end{pmatrix} \cdot \begin{pmatrix} \boldsymbol{F}^{+}(\boldsymbol{k}_{\mathrm{t}}, z) \\ \boldsymbol{F}^{-}(\boldsymbol{k}_{\mathrm{t}}, z) \end{pmatrix} \tag{2.13}$$

where explicit expressions for $\mathbf{Z}_{\mathrm{r}}^{-1}$ and $\mathbf{Z}_{\mathrm{r}}$ are given by (D.1) and (D.2), respectively, in Appendix D.

2.5 Reflection and transmission dyadics

The reflection and transmission dyadics are found from the formal solution to the scattering problem expressed by the propagator dyadic in (2.9). Combination of (2.9) and the wave splitting relations (2.12) and (2.13) for an arbitrary material a on the left and material b on the right, gives the scattering relation

$$\begin{pmatrix} \boldsymbol{F}^{+}(\boldsymbol{k}_{\mathrm{t}}, z_{N-1}) \\ \boldsymbol{F}^{-}(\boldsymbol{k}_{\mathrm{t}}, z_{N-1}) \end{pmatrix} = \mathbf{W} \cdot \begin{pmatrix} \boldsymbol{F}^{+}(\boldsymbol{k}_{\mathrm{t}}, z_1) \\ \boldsymbol{F}^{-}(\boldsymbol{k}_{\mathrm{t}}, z_1) \end{pmatrix} \tag{2.14}$$

where

$$\mathbf{W} = \begin{pmatrix} \mathbf{W}_{11} & \mathbf{W}_{12} \\ \mathbf{W}_{21} & \mathbf{W}_{22} \end{pmatrix} = \frac{1}{2} \begin{pmatrix} \mathbf{I}_2 & -\mathbf{Z}_{\mathrm{r,b}} \\ \mathbf{I}_2 & \mathbf{Z}_{\mathrm{r,b}} \end{pmatrix} \cdot \begin{pmatrix} \mathbf{P}_{11} & \mathbf{P}_{12} \\ \mathbf{P}_{21} & \mathbf{P}_{22} \end{pmatrix} \cdot \begin{pmatrix} \mathbf{I}_2 & \mathbf{I}_2 \\ -\mathbf{Z}_{\mathrm{r,a}}^{-1} & \mathbf{Z}_{\mathrm{r,a}}^{-1} \end{pmatrix} \tag{2.15}$$

Recall that the generating sources are assumed being located in the half-space $z < z_0 < z_1$, as depicted in Figure 1. Thus, the assumption of no sources on the right-hand side of the slab implies $\boldsymbol{F}^-(\boldsymbol{k}_\mathrm{t}, z_{N-1}) = \mathbf{0}$ and the reflection and transmission dyadics with excitation from the left are defined by

$$\begin{cases} \boldsymbol{F}^-(\boldsymbol{k}_\mathrm{t}, z_1) = \mathbf{r}^+ \cdot \boldsymbol{F}^+(\boldsymbol{k}_\mathrm{t}, z_1) \\ \boldsymbol{F}^+(\boldsymbol{k}_\mathrm{t}, z_{N-1}) = \mathbf{t}^+ \cdot \boldsymbol{F}^+(\boldsymbol{k}_\mathrm{t}, z_1) \end{cases} \tag{2.16}$$

where the expressions for $\mathbf{r}^+$ and $\mathbf{t}^+$ in terms of the blocks of (2.15) are [9, 30]

$$\begin{cases} \mathbf{r}^+ = -\mathbf{W}_{22}^{-1} \cdot \mathbf{W}_{21} \\ \mathbf{t}^+ = \mathbf{W}_{11} + \mathbf{W}_{12} \cdot \mathbf{r}^+ \end{cases} \tag{2.17}$$

In case of a PEC backed slab, the boundary conditions make it more convenient to express the fields at the boundary z_{N-1} in terms of the total fields

$$\begin{pmatrix} \mathbf{0} \\ -\eta_0 \boldsymbol{J}_\mathrm{S} \end{pmatrix} = \begin{pmatrix} \boldsymbol{E}_\mathrm{t}(\boldsymbol{k}_\mathrm{t}, z_{N-1}) \\ \eta_0 \mathbf{J} \cdot \boldsymbol{H}_\mathrm{t}(\boldsymbol{k}_\mathrm{t}, z_{N-1}) \end{pmatrix} = \mathbf{T} \cdot \begin{pmatrix} \boldsymbol{F}^+(\boldsymbol{k}_\mathrm{t}, z_1) \\ \boldsymbol{F}^-(\boldsymbol{k}_\mathrm{t}, z_1) \end{pmatrix} \tag{2.18}$$

where $\boldsymbol{J}_\mathrm{S}$ is the surface current density at $z = z_{N-1}$, with $\mathbf{T}$ defined by

$$\mathbf{T} = \mathbf{P}(z_{N-1}, z_1) \cdot \begin{pmatrix} \mathbf{I}_2 & \mathbf{I}_2 \\ -\mathbf{Z}_{\mathrm{r,a}}^{-1} & \mathbf{Z}_{\mathrm{r,a}}^{-1} \end{pmatrix} \tag{2.19}$$

In this case we obtain the reflection and conductance dyadics, $\mathbf{r}^+$ and $\mathbf{g}^+$, respectively, by

$$\begin{cases} \mathbf{r}^+ = -\mathbf{T}_{12}^{-1} \cdot \mathbf{T}_{11} \\ \mathbf{g}^+ = \mathbf{T}_{21} - \mathbf{T}_{22} \cdot \mathbf{r}^+ \end{cases} \tag{2.20}$$

where the conductance dyadic is related to the electric surface current density on the PEC surface for left excitation through [9]

$$-\eta_0 \boldsymbol{J}_\mathrm{S} = \mathbf{g}^+ \cdot \boldsymbol{F}^+(\boldsymbol{k}_\mathrm{t}, z_1) \tag{2.21}$$

Usually, only the reflection dyadic $\mathbf{r}^+$ is of interest.

3 Motivation for the need of a stabilization scheme

The wave propagator formalism is inherently unstable, as pointed out in the Introduction. This section considers this characteristic of the method in more detail and it is shown that numerical breakdown can occur when evanescent wave fields are present in the scattering problem. Numerical examples are presented in order to illustrate and motivate the need for introducing a stabilization scheme in the formulation. At the end of this section, the wave and scattering matrix forms are discussed.

3.1 Origin of numerical instabilities

The fundamental dyadic $\mathbf{M}$ has eigenvectors and eigenvalues $\{\boldsymbol{v}_m, n_m\}_{m=1}^4$

$$\mathbf{M} \cdot \boldsymbol{v}_m = n_m \boldsymbol{v}_m \tag{3.1}$$

where the eigenvalues n_m are the refractive indices of the propagating modes, which have polarizations given by the eigenvectors $\boldsymbol{v}_m$. The propagator has the same eigenvectors and propagation factors as eigenvalues

$$\mathbf{P} \cdot \boldsymbol{v}_m = \mathrm{e}^{\mathrm{i}k_0 n_m d} \boldsymbol{v}_m \tag{3.2}$$

where d is the thickness of the slab, and the quantity $n_m d$ is often referred to as the optical thickness. Note that in lossless isotropic media we would typically have two waves of different polarizations, transverse electric (TE) and transverse magnetic (TM), propagating in each direction, with two positive refractive indices corresponding to waves propagating in the $+z$ direction, and two negative refractive indices corresponding to waves propagating the $-z$ direction. However, since we are dealing with general bianisotropic media and complex-valued refractive indices, we refrain from exploiting this in our notation and simply label all refractive indices by n_m.

We can now see the origin of the numerical instabilities when one or several of the eigenvalues n_m become complex, *i.e.*, the wave modes become evanescent: the exponential function in (3.2) will become either very large or very small as $k_0 d$ becomes large. Thus, in this situation, similar to what was early reported in [6], the elements of the propagator become dominated by the exponentially growing waves, and those of the decaying waves which contain the essential physics, are lost in the computation.

3.2 Illustrations by numerical examples

As argued in the preceding subsection, evanescent wave modes inside a slab or any stratified structure can cause numerical breakdown of the wave propagation algorithm, see *e.g.*, [6, 12, 13, 15, 19, 24, 36]. This subsection illustrates the problem by showing a number of situations where instabilities occur unless a stabilization scheme is applied. All examples presented in this section have been computed in matlab where the `expm` command was used to evaluate the propagator $\mathbf{P}$. Other options are possible *e.g.*, spectral decomposition by use of `diag`, that may result in slightly different numerical performance, with unessential impact on the main results.

3.2.1 Orthogonal basis

In isotropic regions, the wave modes are either homogeneous, obliquely propagating plane waves or inhomogeneous (evanescent) plane waves depending on whether the tangential wave number, k_{t}, is less or greater than the wave number in the material, k. It is common to introduce an angle of incidence (the angle between the incident

wave propagation direction and the normal of the structure), θ_i, through the relation $k_\mathrm{z} = k\cos\theta_\mathrm{i}$, *cf.* (2.4). When evanescent waves are present, *i.e.*, $k_\mathrm{t} > k$, it is often more convenient to use k_z/k than $\cos\theta_\mathrm{i}$.

The transverse wave number $k_\mathrm{t} = \sqrt{k_\mathrm{x}^2 + k_\mathrm{y}^2} = k\sin\theta_\mathrm{i}$ is a non-negative real number, which in general is non-zero, and then it is appropriate to make use of the orthogonal basis defined by

$$\begin{cases} \hat{\boldsymbol{e}}_\parallel(\boldsymbol{k}_\mathrm{t}) = \boldsymbol{k}_\mathrm{t}/k_\mathrm{t} = \hat{\boldsymbol{x}}\cos\phi_\mathrm{i} + \hat{\boldsymbol{y}}\sin\phi_\mathrm{i} \\ \hat{\boldsymbol{e}}_\perp(\boldsymbol{k}_\mathrm{t}) = \hat{\boldsymbol{z}} \times \hat{\boldsymbol{e}}_\parallel(\boldsymbol{k}_\mathrm{t}) = -\hat{\boldsymbol{x}}\sin\phi_\mathrm{i} + \hat{\boldsymbol{y}}\cos\phi_\mathrm{i} \end{cases} \tag{3.3}$$

for the representation of transverse vectors in the x-y-plane. The azimuth angle of incidence ϕ_i is the angle of the tangential wave vector $\boldsymbol{k}_\mathrm{t}$ relative $\hat{\boldsymbol{x}}$. In isotropic media, a wave with the electric field along $\hat{\boldsymbol{e}}_\parallel$ is said to be TM-polarized, whereas if the electric field is along $\hat{\boldsymbol{e}}_\perp$ the wave is TE-polarized.

3.2.2 Reflection and transmission

With the sources located on the left-hand side of the structure, the reflection and transmission dyadics are represented in the orthogonal basis by

$$\begin{cases} \mathbf{r}^+ = r^+_{\parallel\parallel}\hat{\boldsymbol{e}}_\parallel\hat{\boldsymbol{e}}_\parallel + r^+_{\parallel\perp}\hat{\boldsymbol{e}}_\parallel\hat{\boldsymbol{e}}_\perp + r^+_{\perp\parallel}\hat{\boldsymbol{e}}_\perp\hat{\boldsymbol{e}}_\parallel + r^+_{\perp\perp}\hat{\boldsymbol{e}}_\perp\hat{\boldsymbol{e}}_\perp \\ \mathbf{t}^+ = t^+_{\parallel\parallel}\hat{\boldsymbol{e}}_\parallel\hat{\boldsymbol{e}}_\parallel + t^+_{\parallel\perp}\hat{\boldsymbol{e}}_\parallel\hat{\boldsymbol{e}}_\perp + t^+_{\perp\parallel}\hat{\boldsymbol{e}}_\perp\hat{\boldsymbol{e}}_\parallel + t^+_{\perp\perp}\hat{\boldsymbol{e}}_\perp\hat{\boldsymbol{e}}_\perp \end{cases} \tag{3.4}$$

where the first and second subscripts of the coefficients denote the polarization states of the reflected (transmitted) and incident waves, respectively.

The reflected and transmitted power densities, including the cross polarized scattering components, are given by the reflectance and transmittance, R^+ and T^+, respectively. These are in turn given by quadratic expressions of the components of the reflection and transmission dyadics (3.4) as

$$\begin{cases} R^+ = |r^+_{\parallel\parallel}\sin\chi + r^+_{\parallel\perp}\cos\chi/\cos\theta_i|^2 + |r^+_{\perp\parallel}\cos\theta_i\sin\chi + r^+_{\perp\perp}\cos\chi|^2 \\ T^+ = |t^+_{\parallel\parallel}\sin\chi + t^+_{\parallel\perp}\cos\chi/\cos\theta_i|^2 + |t^+_{\perp\parallel}\cos\theta_i\sin\chi + t^+_{\perp\perp}\cos\chi|^2 \end{cases} \tag{3.5}$$

where θ_i is the angle of incidence and χ is the polarization angle, $\chi = 0$ (TE polarization) and $\chi = \pi/2$ (TM polarization). For details, see [9, 29]. However, the expressions (3.5) are limited to the case of equal environments enclosing the structure. To this end one can alternatively apply the more general expressions given by

$$R^+ = \frac{(\mathbf{r}^+\cdot\boldsymbol{E}_0)^*\cdot\mathbf{Z}^{-1}_{\mathrm{r,a}}\cdot\mathbf{r}^+\cdot\boldsymbol{E}_0}{\boldsymbol{E}_0^*\cdot\mathbf{Z}^{-1}_{\mathrm{r,a}}\cdot\boldsymbol{E}_0} \quad \text{and} \quad R^- = \frac{(\mathbf{r}^-\cdot\boldsymbol{E}_0)^*\cdot\mathbf{Z}^{-1}_{\mathrm{r,b}}\cdot\mathbf{r}^-\cdot\boldsymbol{E}_0}{\boldsymbol{E}_0^*\cdot\mathbf{Z}^{-1}_{\mathrm{r,b}}\cdot\boldsymbol{E}_0} \tag{3.6}$$

$$T^+ = \frac{(\mathbf{t}^+\cdot\boldsymbol{E}_0)^*\cdot\mathbf{Z}^{-1}_{\mathrm{r,b}}\cdot\mathbf{t}^+\cdot\boldsymbol{E}_0}{\boldsymbol{E}_0^*\cdot\mathbf{Z}^{-1}_{\mathrm{r,a}}\cdot\boldsymbol{E}_0} \quad \text{and} \quad T^- = \frac{(\mathbf{t}^-\cdot\boldsymbol{E}_0)^*\cdot\mathbf{Z}^{-1}_{\mathrm{r,a}}\cdot\mathbf{t}^-\cdot\boldsymbol{E}_0}{\boldsymbol{E}_0^*\cdot\mathbf{Z}^{-1}_{\mathrm{r,b}}\cdot\boldsymbol{E}_0} \tag{3.7}$$

where $*$ denotes the complex conjugate, $\mathbf{Z}_{\mathrm{r,a}}^{-1}$ and $\mathbf{Z}_{\mathrm{r,b}}^{-1}$ are the relative wave admittance operators of medium a on the left and medium b on the right, respectively, see Appendix D, and $\boldsymbol{E}_0$ is the polarization defined by

$$\boldsymbol{E}_0 = \hat{\boldsymbol{e}}_{\parallel} \sin\chi + \hat{\boldsymbol{e}}_{\perp} \cos\chi$$

which can also be given a cartesian representation in a global coordinate system, $\boldsymbol{E}_0 = E_x\hat{\boldsymbol{x}} + E_y\hat{\boldsymbol{y}}$, depending on which is most convenient.

3.2.3 Dielectric slab with losses

Our first case is a lossy dielectric material of thickness d enclosed by free space. Due to the losses, the wave number in the material has an imaginary part causing an exponentially decreasing/increasing wave propagation factor. The slab is assumed being isotropic with relative material parameters given by

$$\boldsymbol{\epsilon} = (1+\mathrm{i})\mathbf{I}_3, \quad \boldsymbol{\mu} = \mu\mathbf{I}_3, \quad \boldsymbol{\xi} = \boldsymbol{\zeta} = \mathbf{0} \tag{3.8}$$

The eigenvalues of the fundamental dyadic are

$$n^2 = \epsilon\mu - k_{\mathrm{t}}^2/k_0^2 \tag{3.9}$$

Thus, the refractive index in the material has an imaginary part $\operatorname{Im} n_m \neq 0$, causing an exponentially decreasing/increasing wave propagation factor, *cf.* Section 3.1. Figure 2 shows results for the computed reflectance and transmittance, by use of the standard propagator formulation in [9, 29]. It is clearly seen that numerical instabilities occur for thick slabs, indicated by the strong oscillations and above-unity results that start at $k_0 d \approx 60$. Thus, the type of instability is associated with attenuated fields due to absorption in lossy layers that have high thickness/wavelength ratio [15].

3.2.4 Frustrated total internal reflection

When a plane wave in a dense medium is incident at a sufficiently large angle on a less dense medium, we have the situation of a real longitudinal wave number k_{z} in the dense medium, and an imaginary one in the less dense (with exponential attenuation of evanescent waves). When only two media are present, this leads to total internal reflection, and zero transmission. However, even though there is exponential attenuation, there are still some electromagnetic fields in the less dense medium (having evanescent waves). If a second interface is brought close enough to the first interface, a positive power transfer through the coupling of evanescent waves in both directions may occur (tunneling). This typically happens when the distance is significantly less than the wavelength in free space.

Results are shown in Figure 3 for an air slab enclosed by isotropic dielectric materials a and b with refractive indices $n_{\mathrm{a}} = n_{\mathrm{b}} = 2$. The air slab has material parameters

$$\boldsymbol{\epsilon} = \mathbf{I}_3, \quad \boldsymbol{\mu} = \mu\mathbf{I}_3, \quad \boldsymbol{\xi} = \boldsymbol{\zeta} = \mathbf{0} \tag{3.10}$$

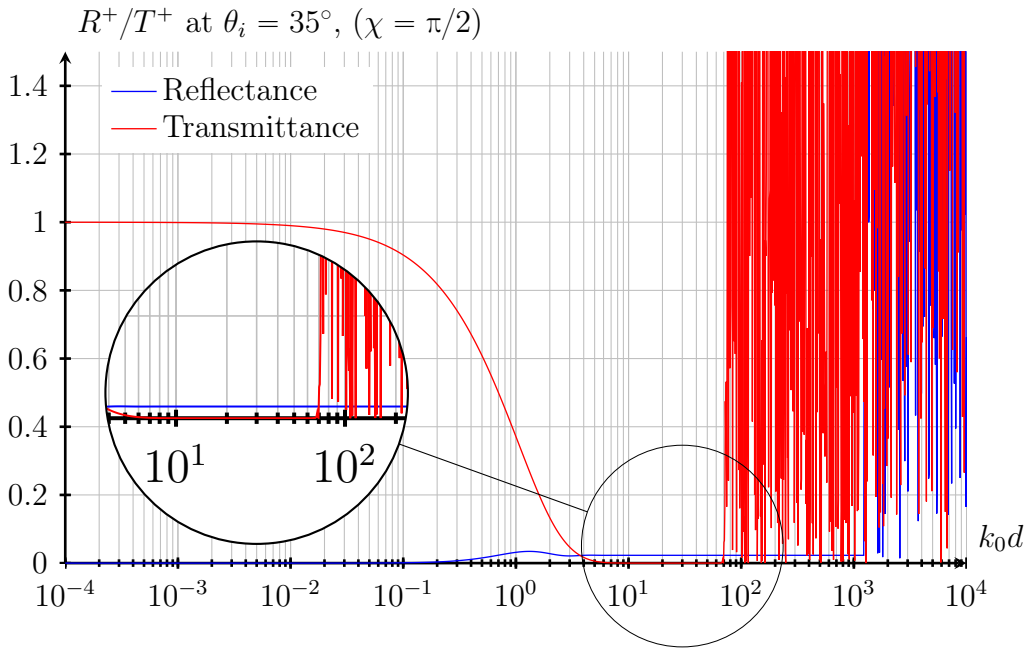

Figure 2: The reflectance and transmittance (TM polarization) by use of the standard propagator formulation in [9, 29], for the lossy isotropic slab at angle of incidence $\theta_{\rm i} = 35^\circ$.

Figure 3 shows results from computed reflectance and transmittance by use of the same technique as the preceding example *i.e.*, without use of any stabilization scheme. Note that for very small $k_0 d$, there is high transmittance and low reflectance, which changes to low transmittance and high reflectance around $k_0 d \approx 1$. The numerical instabilities start at $kd \approx 60$. For details and derivation of the correspondence between the electromagnetic analog of quantum mechanical tunneling by use of the transfer matrix approach, see [28].

3.2.5 Non-magnetic lossless gyrotropic slab

When a plasma (a collection of free floating charged particles) is subjected to a magnetic field, a gyrotropic material model is applicable. The eigenwaves of this material are circularly polarized with respect to the axis of the magnetic field. With a sufficiently strong magnetic field, one of the eigenwaves may have an imaginary wave number, causing exponential attenuation or increase. A non-magnetic gyrotropic lossless material is modeled by the constitutive relations (where the notation $[\boldsymbol{\epsilon}]$ is used for a matrix representation of the dyadic $\boldsymbol{\epsilon}$ in the xyz coordinate system)

$$[\boldsymbol{\epsilon}] = \begin{pmatrix} \epsilon_{\rm r} & {\rm i}\epsilon_{\rm g} & 0 \\ -{\rm i}\epsilon_{\rm g} & \epsilon_{\rm r} & 0 \\ 0 & 0 & \epsilon_{\rm z} \end{pmatrix}, \quad \boldsymbol{\mu} = \mathbf{I}_3, \quad \boldsymbol{\xi} = \boldsymbol{\zeta} = \mathbf{0} \tag{3.11}$$

where $\epsilon_{\rm r}$, $\epsilon_{\rm g}$ and $\epsilon_{\rm z}$ are real numbers, with $\epsilon_{\rm r}$ and $\epsilon_{\rm z}$ being non-negative. At normal incidence, $k_{\rm t} = 0$, it can be shown that the eigenvalues of the fundamental matrix

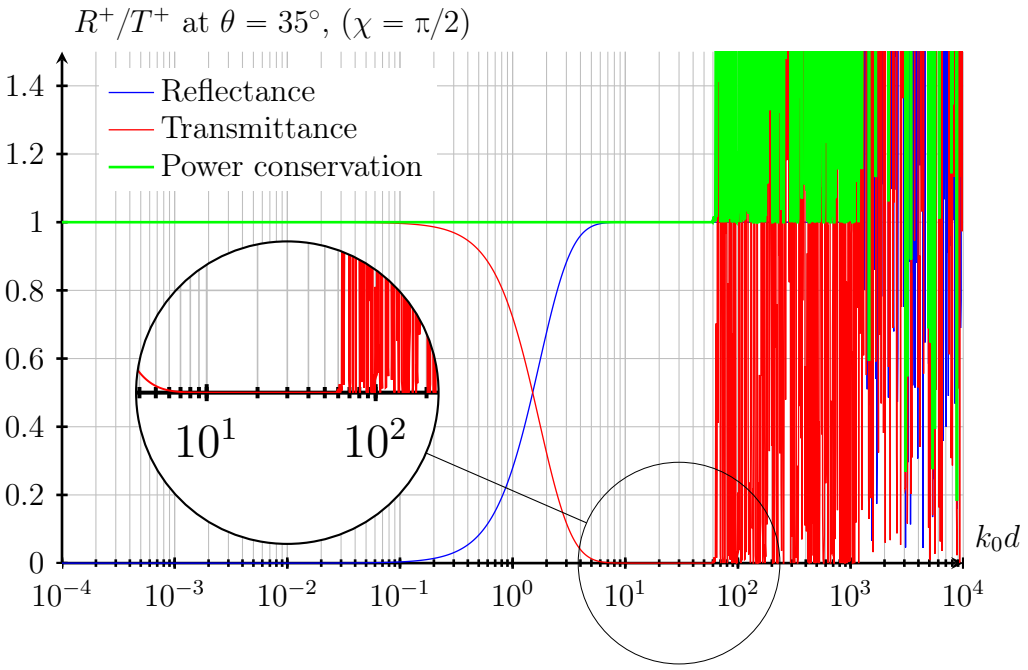

Figure 3: The reflectance and transmittance (TM polarization)by use of the standard propagator formulation in [9, 29], for the air slab enclosed by isotropic dielectric materials distinct from vacuum, at angle of incidence $\theta = 35^\circ$.

M are

$$n_{\pm}^2 = \epsilon_{\mathrm{r}} \pm \epsilon_{\mathrm{g}} \tag{3.12}$$

Thus, there exists a wave number in the material, with imaginary part $\operatorname{Im} n_m \neq 0$, if $|\epsilon_{\mathrm{g}}| > \epsilon_{\mathrm{r}}$, causing exponentially decreasing/increasing wave propagation factors.

For reference and verification purposes, we list below analytical expressions for the reflection and transmission dyadics in case of normal incidence on a gyrotropic slab, which can be found by explicit calculations using the eigenvectors and eigenvalues of **M**. The results for cases without and with PEC-backing are given in the following paragraphs.

Slab enclosed by air The reflection and transmission coefficients for a slab enclosed by air at normal incidence are

$$\begin{cases} r_{\parallel}^{+} = -\dfrac{(1+\frac{\tan(\xi n_+)}{\mathrm{i}n_+})(1+\frac{\tan(\xi n_-)}{\mathrm{i}n_-}) - (1-\mathrm{i}n_+\tan(\xi n_+)(1-\mathrm{i}n_-\tan(\xi n_-)}{4(1+\frac{\tan(\xi n_+)}{2\mathrm{i}n_+}(1+n_+^2))(1+\frac{\tan(\xi n_-)}{2\mathrm{i}n_-}(1+n_-^2))} \\ r_{\perp}^{+} = -\dfrac{\frac{\tan(\xi n_+)}{n_+}(1-n_+^2)}{4(1+\frac{\tan(\xi n_+)}{2\mathrm{i}n_+}(1+n_+^2))} + \dfrac{\frac{\tan(\xi n_-)}{n_-}(1-n_-^2)}{4(1+\frac{\tan(\xi n_-)}{2\mathrm{i}n_-}(1+n_-^2))} \\ t_{\parallel}^{+} = \dfrac{1}{2(\cos(\xi n_+)+\frac{\sin(\xi n_+)}{2\mathrm{i}n_+}(1+n_+^2))} + \dfrac{1}{2(\cos(\xi n_-)+\frac{\sin(\xi n_-)}{2\mathrm{i}n_-}(1+n_-^2))} \\ t_{\perp}^{+} = \dfrac{1}{2\mathrm{i}(\cos(\xi n_+)+\frac{\sin(\xi n_+)}{2\mathrm{i}n_+}(1+n_+^2))} - \dfrac{1}{2\mathrm{i}(\cos(\xi n_-)+\frac{\sin(\xi n_-)}{2\mathrm{i}n_-}(1+n_-^2))} \end{cases} \tag{3.13}$$

where $\xi = k_0 d$ is the phase thickness of the slab, and $n_\pm$ are given by (3.12). The reflection and transmission dyadics are

$$\begin{cases} \mathbf{r}^{+} = r_{\parallel}^{+}\mathbf{I}_2 + r_{\perp}^{+}\mathbf{J} \\ \mathbf{t}^{+} = t_{\parallel}^{+}\mathbf{I}_2 + t_{\perp}^{+}\mathbf{J} \end{cases} \tag{3.14}$$

where $\mathbf{J} = \hat{\boldsymbol{z}} \times \mathbf{I}_2 = \hat{\boldsymbol{z}} \times (\hat{\boldsymbol{e}}_{\parallel}\hat{\boldsymbol{e}}_{\parallel} + \hat{\boldsymbol{e}}_{\perp}\hat{\boldsymbol{e}}_{\perp}) = \hat{\boldsymbol{e}}_{\perp}\hat{\boldsymbol{e}}_{\parallel} - \hat{\boldsymbol{e}}_{\parallel}\hat{\boldsymbol{e}}_{\perp}$. The co- and cross polarization coefficients $r_{\parallel}^{+}$ ($t_{\parallel}^{+}$) and $r_{\perp}^{+}$ ($t_{\perp}^{+}$), respectively, are related to the coefficients of the reflection (transmission) dyadics (3.4) by $r_{\parallel}^{+} = r_{\parallel\parallel}^{+} = r_{\perp\perp}^{+}$, and $r_{\perp}^{+} = -r_{\parallel\perp}^{+} = r_{\perp\parallel}^{+}$ and similarily for the transmission coefficients.

PEC backed slab The reflection coefficients for a PEC backed slab with air to the left at normal incidence are

$$\begin{cases} r_{\parallel}^{+} - \dfrac{1+\frac{\tan(\xi n_+)}{n_+}\frac{\tan(\xi n_-)}{n_-}}{\left(1-\mathrm{i}\frac{\tan(\xi n_+)}{n_+}\right)\left(1-\mathrm{i}\frac{\tan(\xi n_-)}{n_-}\right)} \\ r_{\perp}^{+} = -\dfrac{\frac{\tan(\xi n_+)}{n_+} - \frac{\tan(\xi n_-)}{n_-}}{\left(1-\mathrm{i}\frac{\tan(\xi n_+)}{n_+}\right)\left(1-\mathrm{i}\frac{\tan(\xi n_-)}{n_-}\right)} \end{cases} \tag{3.15}$$

with the reflection dyadic of the form

$$\mathbf{r}^{+} = r_{\parallel}^{+}\mathbf{I}_2 + r_{\perp}^{+}\mathbf{J} \tag{3.16}$$

The reflectance and transmittance for a gyrotropic slab enclosed by air is depicted in Figure 4, which shows that the degradation of numerical accuracy starts at $kd \approx 5$. Furthermore, Figure 5 presents $|r_{\parallel}^{+}|$, for the case of a PEC-backed lossless gyrotropic slab, showing that the instabilities start at $kd \approx 5$ also for this case, similar to the results reported in [36].

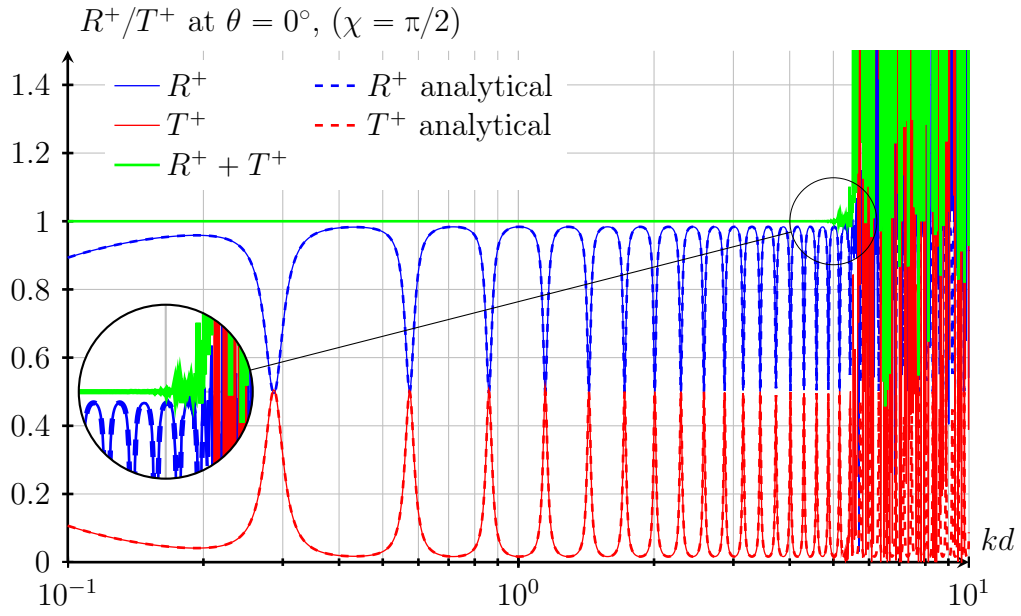

Figure 4: The reflectance and transmittance at normal incidence by use of the standard propagator formulation in [9, 29], and the analytical expressions (3.13) and (3.14), for a lossless gyrotropic slab enclosed by air, with $\epsilon_{\rm r} = 40$ and $\epsilon_{\rm g} = 80$.

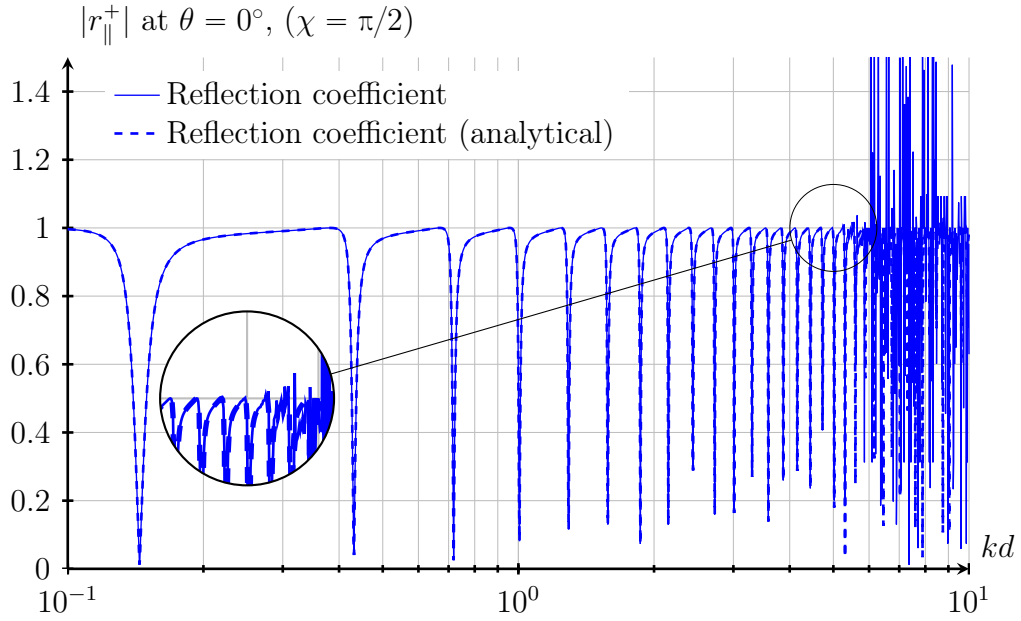

Figure 5: The co-polarized reflection coefficient at normal incidence by use of the standard propagator formulation in [9, 29], and the analytical expressions (3.15) and (3.16), for a PEC-backed lossless gyrotropic slab with $\epsilon_{\rm r} = 40$ and $\epsilon_{\rm g} = 80$, [36].

3.2.6 Dispersive bianisotropic slab

This example considers a PEC backed dispersive chiro-omega medium enclosed by vacuum, as an example of an anti-reflection surface optimized for low reflection within a given frequency band, see [20]. The chiro-omega medium is an example of a bianisotropic medium. This example illustrates that a slight perturbation of a material parameter can cause loss of accuracy without the use of any stabilization scheme of the propagator formalism.

More specifically, the permittivity and permeability dyadics $\boldsymbol{\epsilon}$ and $\boldsymbol{\mu}$ of the slab are given by the matrix representations [20]

$$[\boldsymbol{\epsilon}] = \begin{pmatrix} \epsilon_{\mathrm{t}} & 0 & 0 \\ 0 & \epsilon_{\mathrm{t}} & 0 \\ 0 & 0 & \epsilon_{\mathrm{zz}} \end{pmatrix} \qquad [\boldsymbol{\mu}] = \begin{pmatrix} \mu_{\mathrm{t}} & 0 & 0 \\ 0 & \mu_{\mathrm{t}} & 0 \\ 0 & 0 & \mu_{\mathrm{zz}} \end{pmatrix} \tag{3.17}$$

where

$$\begin{cases} \epsilon_{\mathrm{t}} = \epsilon_{\mathrm{r}}\big(1 + \dfrac{\omega_{\mathrm{p}}^2}{\omega_0^2 - \omega^2 - (\omega_{\mathrm{p}}^2 + A^2\omega^2)/3 - i2\nu\omega}\big) \\ \epsilon_{\mathrm{zz}} = \epsilon_{\mathrm{r}} \\ \mu_{\mathrm{t}} = \mu_{\mathrm{r}}\big(1 + \dfrac{A^2\omega^2}{\omega_0^2 - \omega^2 - (\omega_{\mathrm{p}}^2 + A^2\omega^2)/3 - i2\nu\omega}\big) \\ \mu_{\mathrm{zz}} = \mu_{\mathrm{r}} \end{cases} \tag{3.18}$$

The other two coupling dyadics, $\boldsymbol{\xi}$ and $\boldsymbol{\zeta}$ are [21]

$$[\boldsymbol{\xi}] = \begin{pmatrix} \mathrm{i}\kappa & \mathrm{i}\Omega & 0 \\ -\mathrm{i}\Omega & \mathrm{i}\kappa & 0 \\ 0 & 0 & 0 \end{pmatrix} \qquad [\boldsymbol{\zeta}] = \begin{pmatrix} -\mathrm{i}\kappa & \mathrm{i}\Omega & 0 \\ -\mathrm{i}\Omega & -\mathrm{i}\kappa & 0 \\ 0 & 0 & 0 \end{pmatrix} \tag{3.19}$$

where

$$\begin{cases} \kappa = \dfrac{\sqrt{\epsilon_{\mathrm{r}}\mu_{\mathrm{r}}}\omega_{\mathrm{p}} A\omega \sin\beta}{\omega_0^2 - \omega^2 - (\omega_{\mathrm{p}}^2 + A^2\omega^2)/3 - i2\nu\omega} \\ \Omega = \dfrac{\sqrt{\epsilon_{\mathrm{r}}\mu_{\mathrm{r}}}\omega_{\mathrm{p}} A\omega \cos\beta}{\omega_0^2 - \omega^2 - (\omega_{\mathrm{p}}^2 + A^2\omega^2)/3 - i2\nu\omega} \end{cases} \tag{3.20}$$

Figures 6 and 7 show the real and imaginary parts of the material variables corresponding to $\boldsymbol{\epsilon}$, $\boldsymbol{\mu}$, $\boldsymbol{\xi}$ and $\boldsymbol{\zeta}$, respectively. Notice that data for a perturbed slab, where A is changed from 0.353 to 0.553, are included for the purpose of comparison.

Figure 8 shows results from computed reflectance for the PEC backed bianisotropic slab and its perturbed counterpart. It is seen in Figure 8 that numerical instabilities occur in the case of the perturbed slab, within the frequency band where the slab exhibits strong dispersion, *i.e.*, between 9 and 10 GHz. Thus, this example illustrates the fact that a stabilization scheme is needed in order to get accurate results, which is critical if the propagator method is intended to be used in combination with, *e.g.*, an optimization algorithm for the design of devices that exhibit strong dispersion.

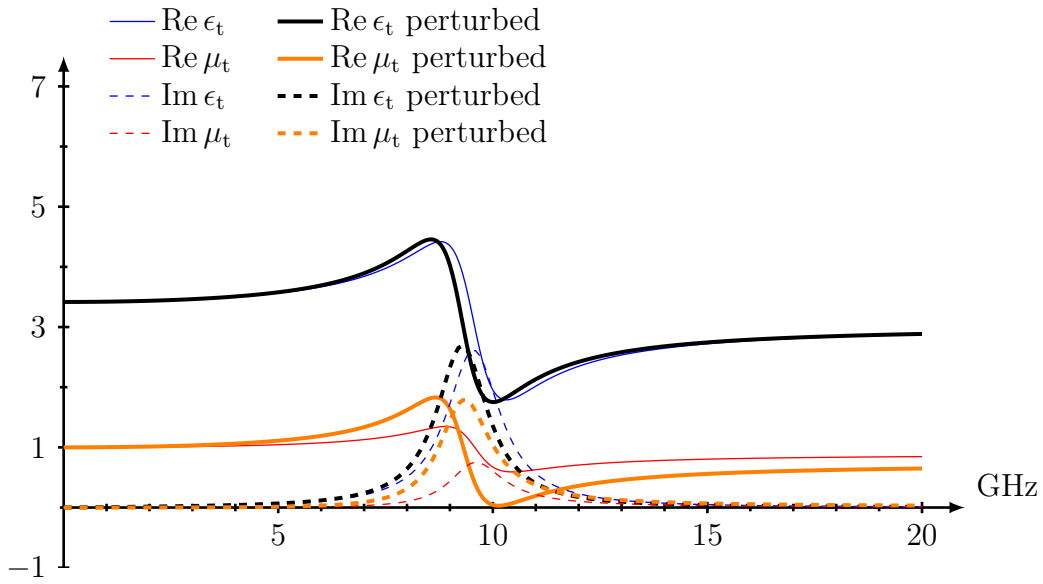

Figure 6: Real and imaginary parts of the variables (3.18) of $\boldsymbol{\epsilon}$ and $\boldsymbol{\mu}$, with parameters in accordance with paper VII in [21], *i.e.*, with $\epsilon_r = 3$, $\mu_r = 1$, $f_0 = 10$ GHz, $\omega_0 = 2\pi f_0$, $\omega_p = 2.29 \cdot 10^{10}$, $\nu = 5$ GHz, $\beta = 48.0°$ and $A = 0.353$. The material parameters of the perturbed slab were identical, except A that was given the value 0.553.

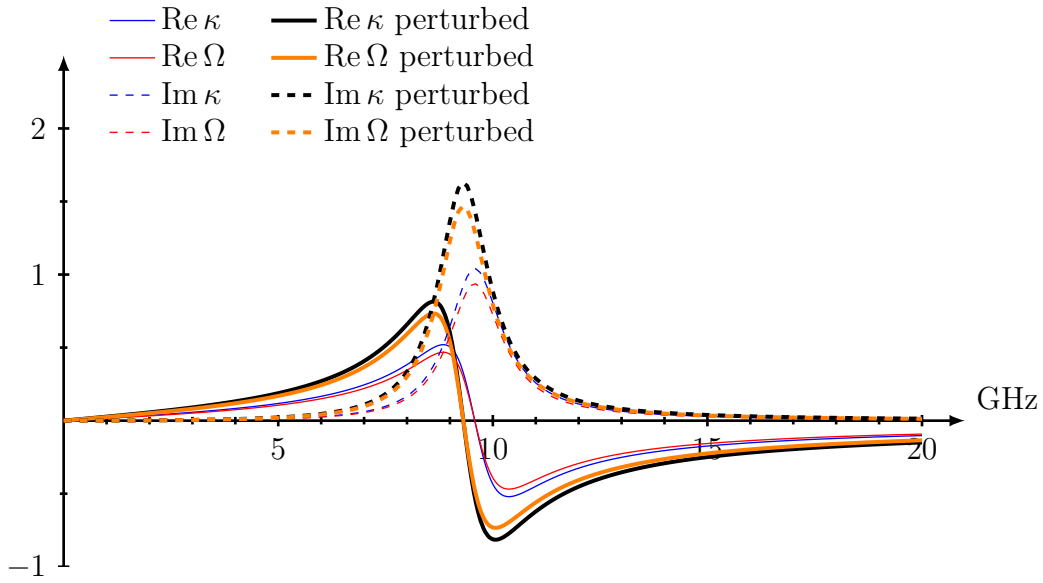

Figure 7: Real and imaginary parts of the variables (3.20) of $\boldsymbol{\xi}$ and $\boldsymbol{\zeta}$, with parameters in accordance with paper VII in [21], *i.e.*, with $\epsilon_r = 3$, $\mu_r = 1$, $f_0 = 10$ GHz, $\omega_0 = 2\pi f_0$, $\omega_p = 2.29 \cdot 10^{10}$, $\nu = 5$ GHz, $\beta = 48.0°$ and $A = 0.353$. The material parameters of the perturbed slab were identical, except A that was given the value 0.553.

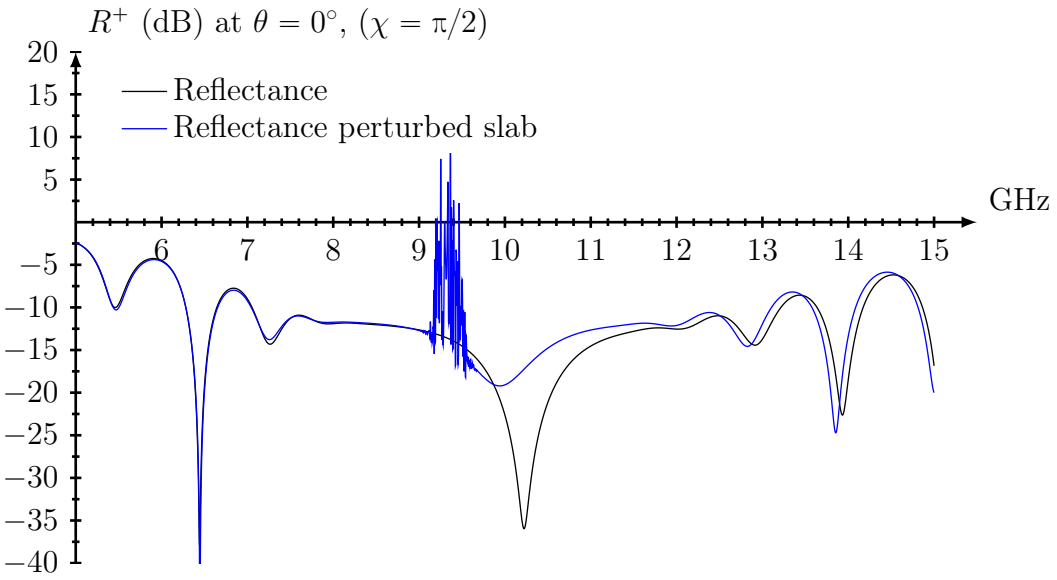

Figure 8: Reflectance at normal incidence from a PEC backed dispersive bianisotropic slab of thickness 60 mm, enclosed by vacuum. The values of the constitutive dyadic $\boldsymbol{\epsilon}$, $\boldsymbol{\mu}$, $\boldsymbol{\xi}$ and $\boldsymbol{\zeta}$ in (3.17) and (3.19) are specified in Figure 6 and 7, respectively.

3.2.7 Periodic bandgap structure

Define a unit cell structure, consisting of two isotropic materials having high and low refractive indices n_{H} and n_{L}, respectively, and thicknesses d_{H} and d_{L}. By stacking a number of unit cells in sequence, it is well known that a stop band with very low transmission may occur. When choosing the optical thickness $n_{\mathrm{H}}d_{\mathrm{H}} = n_{\mathrm{L}}d_{\mathrm{L}} = \lambda_0/4$, where λ_0 is the free space wavelength at design frequency f_0, the result is a stop band centered at f_0 with a bandwidth determined by the contrast $n_{\mathrm{H}}/n_{\mathrm{L}}$.

Inspired by Chapter 6 in [22] on dielectric mirrors, we assume that the periodic structure has an odd number of layers, with the high index layer n_{H} being the first and last layer. More specifically, we assume $n_{\mathrm{L}} = 1.38$, $n_{\mathrm{H}} = 2.32$ and choose a structure made of 70 periods, *i.e.*, in total 141 layers. Figure 9 shows results in the case of the structure being enclosed by isotropic dielectric materials a and b, with refractive indices $n_{\mathrm{a}} = 1$ and $n_{\mathrm{b}} = 1.52$, *i.e.*, vacuum on the left and an isotropic dielectric material on the right.

In Figure 9, it is seen that numerical instabilities occur with respect to transmission around the center of the stop band, *i.e.*, $\lambda = 500$ nm. This can be explained by the total propagator of the structure being $(\mathbf{P}_{\mathrm{H}} \cdot \mathbf{P}_{\mathrm{L}})^N \cdot \mathbf{P}_{\mathrm{H}}$, where $\mathbf{P}_{\mathrm{H}}$ is the propagator for the high index material, $\mathbf{P}_{\mathrm{L}}$ is the propagator for the low index, and N is the number of unit cells. In the stop band, it can be shown that some of the eigenvalues of the unit cell propagator $\mathbf{P}_{\mathrm{H}} \cdot \mathbf{P}_{\mathrm{L}}$ are not of unit magnitude, and similar problems as in the previous examples with exponentially increasing or decreasing factors occur.

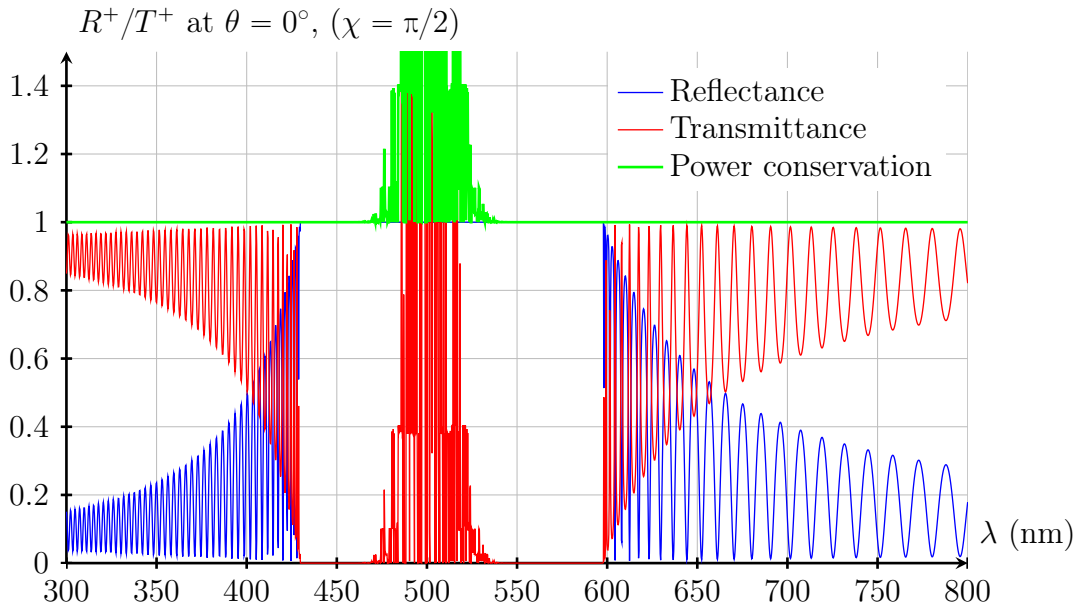

Figure 9: Reflectance and transmittance at normal incidence by use of the standard propagator formulation in [9, 29], for the periodic bandstop structure.

The given examples have shown that care should be taken when evanescent wave modes are present in the scattering problem. The origin of the numerical instabilities, specifically associated with total internal reflection as well as from the imaginary component of the refractive index associated with absorption in layers that have high thickness/wavelength ratio is discussed in more detail in [15]. Furthermore, it was also illustrated that care should be taken for frequencies where strong dispersion occurs.

4 Stable reformulation of the propagator method

This section introduces the main result of the present paper, *i.e.*, a reformulation of the propagator method presented in [9, 30], that solves the reflection as well as the transmission problem in a well-conditioned formulation accomplished by transforming the method into a scattering matrix form in combination with a spectral decomposition of the propagator where exponentially growing and decaying terms are separated. A similar technique has been reported in [6].

4.1 Wave and scattering matrix relations

The propagator method is on a transfer matrix form, *i.e.*, based on wave propagation operators that map the total tangential electric and magnetic fields through a stack of material layers, *cf.* (2.9). Using a wave splitting, see Section 2.4, transforms the propagator formulation into a wave matrix form, *cf.* (2.14), that relates the forward

and backward propagating electric waves [26].

As illustrated in Figure 10, the wave matrix formulation relates the input and output wave fields in accordance with

$$\begin{pmatrix} \boldsymbol{F}^+(\boldsymbol{k}_\mathrm{t}, z_{N-1}) \\ \boldsymbol{F}^-(\boldsymbol{k}_\mathrm{t}, z_{N-1}) \end{pmatrix} = \mathbf{W} \cdot \begin{pmatrix} \boldsymbol{F}^+(\boldsymbol{k}_\mathrm{t}, z_1) \\ \boldsymbol{F}^-(\boldsymbol{k}_\mathrm{t}, z_1) \end{pmatrix} = \begin{pmatrix} \mathbf{W}_{11} & \mathbf{W}_{12} \\ \mathbf{W}_{21} & \mathbf{W}_{22} \end{pmatrix} \cdot \begin{pmatrix} \boldsymbol{F}^+(\boldsymbol{k}_\mathrm{t}, z_1) \\ \boldsymbol{F}^-(\boldsymbol{k}_\mathrm{t}, z_1) \end{pmatrix} \tag{4.1}$$

and for the scattering matrix formulation depicted in Figure 11, the relation reads

$$\begin{pmatrix} \boldsymbol{F}^-(\boldsymbol{k}_\mathrm{t}, z_1) \\ \boldsymbol{F}^+(\boldsymbol{k}_\mathrm{t}, z_{N-1}) \end{pmatrix} = \mathbf{S} \cdot \begin{pmatrix} \boldsymbol{F}^+(\boldsymbol{k}_\mathrm{t}, z_1) \\ \boldsymbol{F}^-(\boldsymbol{k}_\mathrm{t}, z_{N-1}) \end{pmatrix} = \begin{pmatrix} \mathbf{S}_{11} & \mathbf{S}_{12} \\ \mathbf{S}_{21} & \mathbf{S}_{22} \end{pmatrix} \cdot \begin{pmatrix} \boldsymbol{F}^+(\boldsymbol{k}_\mathrm{t}, z_1) \\ \boldsymbol{F}^-(\boldsymbol{k}_\mathrm{t}, z_{N-1}) \end{pmatrix} \tag{4.2}$$

Thus, by definition, the W- and S-matrix formulations mainly differ with respect to the relation between the input and output wave fields. However, cascading slabs with the W-matrix form is ordinary matrix multiplication while the S-matrices are cascaded in terms of the star product that is reviewed in Section 5.

It was pointed out in the Introduction, that the propagator method and related methods are inherently unstable, a fact supported by the discussion in Section 3.1. As is illustrated in Figure 10 and seen in (4.1), the wave matrix always propagates the fields in the forward direction when $d = z_{N-1} - z_1 > 0$. It is in fact the arguments of $\mathbf{P}$ that determines the direction of propagation. This implies that wave fields associated with eigenvalues having negative imaginary part will increase when mapped with $\mathbf{W}$, *cf.* the motivation given in Section 3.1. Thus, the existence of evanescent wave fields can render numerical instabilities in layers that have high thickness/wavelength ratio.

The blocks of the scattering matrix (dyadic) $\mathbf{S}$ are by definition the reflection and transmission dyadics $\mathbf{r}^\pm$ and $\mathbf{t}^\pm$, where the $+$ or $-$ sign indicates whether the incident field is propagating in the positive or negative z-direction, respectively. Thus, $\mathbf{S}$ can be rewritten in terms of the wave matrix (dyadic) $\mathbf{W}$ through the transformation [9]

$$\begin{cases} \mathbf{S}_{11} = \mathbf{r}^+ = -\mathbf{W}_{22}^{-1} \cdot \mathbf{W}_{21} \\ \mathbf{S}_{12} = \mathbf{t}^- = \mathbf{W}_{22}^{-1} \\ \mathbf{S}_{21} = \mathbf{t}^+ = \mathbf{W}_{11} + \mathbf{W}_{12} \cdot \mathbf{r}^+ = \mathbf{W}_{11} - \mathbf{W}_{12} \cdot \mathbf{W}_{22}^{-1} \cdot \mathbf{W}_{21} \\ \mathbf{S}_{22} = \mathbf{r}^- = \mathbf{W}_{12} \cdot \mathbf{t}^- = \mathbf{W}_{12} \cdot \mathbf{W}_{22}^{-1} \end{cases} \tag{4.3}$$

where the blocks $\mathbf{S}_{11}$, $\mathbf{S}_{12}$, $\mathbf{S}_{21}$ and $\mathbf{S}_{22}$ have been identified with the reflection and transmission dyadics, *cf.* Section 2.5, hence the name scattering matrix make sense.

The inverse of (4.3) gives the wave matrix $\mathbf{W}$ in terms of the scattering matrix $\mathbf{S}$ *i.e.*,

$$\begin{cases} \mathbf{W}_{11} = \mathbf{S}_{21} - \mathbf{S}_{22} \cdot \mathbf{S}_{12}^{-1} \cdot \mathbf{S}_{11} \\ \mathbf{W}_{12} = \mathbf{S}_{22} \cdot \mathbf{S}_{12}^{-1} \\ \mathbf{W}_{21} = -\mathbf{S}_{12}^{-1} \cdot \mathbf{S}_{11} \\ \mathbf{W}_{22} = \mathbf{S}_{12}^{-1} \end{cases} \tag{4.4}$$

From (4.3) it is clear that $\mathbf{S}$ is not stable if $\mathbf{W}$ is not stable. To this end, in order to obtain a numerically stable formulation, we will instead derive the scattering matrix formulation (4.2) through reformulation of (2.14).

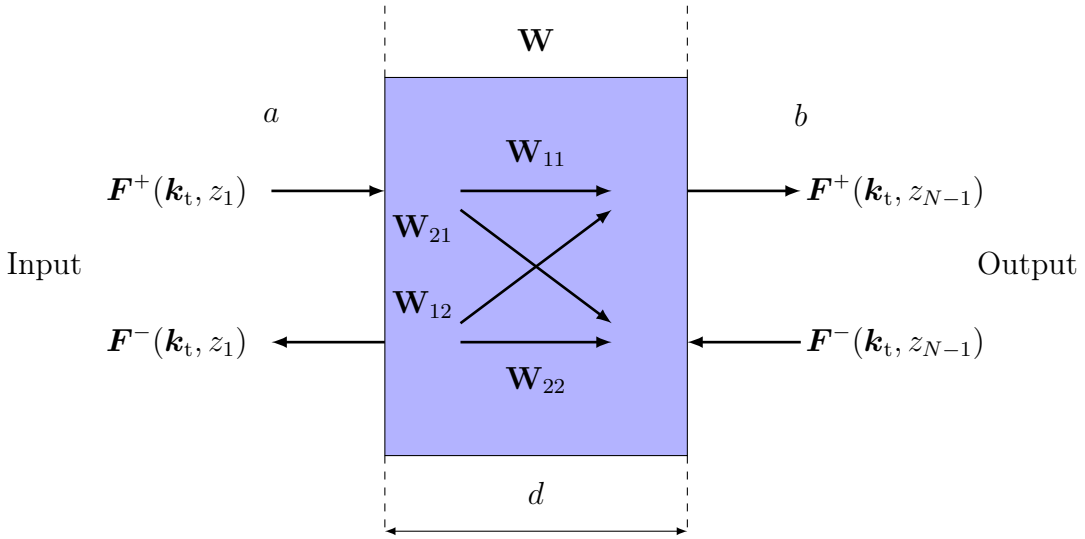

Figure 10: The wave matrix $\mathbf{W}$ for a slab enclosed by two homogeneous isotropic half-spaces a on the left, and b on the right. The total tangential output fields (scattered) $\boldsymbol{F}^+(\boldsymbol{k}_\mathrm{t}, z_{N-1})$ and $\boldsymbol{F}^-(\boldsymbol{k}_\mathrm{t}, z_{N-1})$ consist of waves transmitted through the slab as well as waves reflected from the slab. Outside the slab the wave functions are expressed as a superposition of forward and backward propagating (electric) fields, see Section 2.4.

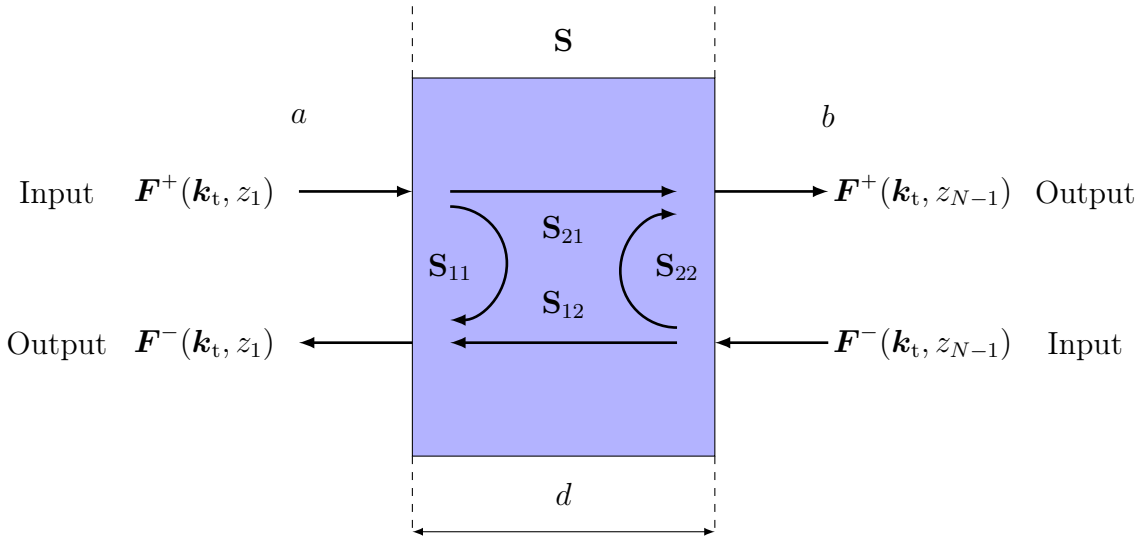

Figure 11: The scattering matrix $\mathbf{S}$ for a slab enclosed by two homogeneous isotropic half-spaces a on the left, and b on the right. The scattering matrix $\mathbf{S}$ relates the total tangential input fields $\boldsymbol{F}^+(\boldsymbol{k}_\mathrm{t}, z_1)$ and $\boldsymbol{F}^-(\boldsymbol{k}_\mathrm{t}, z_{N-1})$ to the output fields $\boldsymbol{F}^-(\boldsymbol{k}_\mathrm{t}, z_1)$ and $\boldsymbol{F}^+(\boldsymbol{k}_\mathrm{t}, z_{N-1})$ *i.e.*, the scattering matrix relates the incident fields to the scattered in any direction. The block matrices $\mathbf{S}_{11}$ and $\mathbf{S}_{22}$ map the reflected backward and forward propagating fields, whereas $\mathbf{S}_{12}$ and $\mathbf{S}_{21}$ map the transmitted backward and forward propagating fields, respectively.

4.2 Spectral decomposition

In the following, we use the left eigenvectors $\boldsymbol{u}_m$ defined by $\boldsymbol{u}_m^* \cdot \mathbf{P} = \mathrm{e}^{\mathrm{i}k_0 dn_m}\boldsymbol{u}_m^*$ rather than the right eigenvectors $\boldsymbol{v}_m$ used in section 3.1. The left eigenvectors can be computed straightforwardly numerically for any given $\mathbf{P}$. For instance, in matlab use `[V,D,U] = eig(M)` to compute right eigenvectors `V`, eigenvalues `D`, and left eigenvectors `U`, whereas in python we could use `scipy.linalg.eig` function with the option `left=True` to make the same computation. Hence, we have

$$\mathbf{U}^\dagger \cdot \mathbf{P} = \mathbf{D} \cdot \mathbf{U}^\dagger \tag{4.5}$$

where $\mathbf{U}$ is a 4×4 matrix with the left eigenvectors as columns, $\dagger$ denotes the Hermitian transpose, $\mathbf{P}$ is the 4×4 matrix representation of the propagator, and $\mathbf{D}$ is a diagonal matrix of eigenvalues

$$\mathbf{D} = \begin{pmatrix} \mathrm{e}^{\mathrm{i}k_0 dn_1} & 0 & 0 & 0 \\ 0 & \mathrm{e}^{\mathrm{i}k_0 dn_2} & 0 & 0 \\ 0 & 0 & \mathrm{e}^{\mathrm{i}k_0 dn_3} & 0 \\ 0 & 0 & 0 & \mathrm{e}^{\mathrm{i}k_0 dn_4} \end{pmatrix} \tag{4.6}$$

The propagator dyadic $\mathbf{P}$ is diagonalizable if it is not defective, *i.e.*, if the eigenvectors still span $\mathbb{C}^4$. More details concerning different representations the propagator $\mathbf{P}$, can be found in Appendix F of [9]. We now proceed to use this spectral decomposition to find a stable formulation for the scattering matrix.

4.3 Transformation into stable scattering matrix form

As a first step in the development of an unconditionally stable formulation, we derive the scattering matrix form (4.2) through reformulation of (2.14). The scattering relation (2.14) for a slab, enclosed by two homogeneous isotropic half-spaces is rewritten as

$$\begin{pmatrix} \mathbf{I}_2 & \mathbf{I}_2 \\ -\mathbf{Z}_{\mathrm{r,b}}^{-1} & \mathbf{Z}_{\mathrm{r,b}}^{-1} \end{pmatrix} \cdot \begin{pmatrix} \boldsymbol{F}_{\mathrm{b}}^{+} \\ \boldsymbol{F}_{\mathrm{b}}^{-} \end{pmatrix} = \mathbf{P} \cdot \begin{pmatrix} \mathbf{I}_2 & \mathbf{I}_2 \\ -\mathbf{Z}_{\mathrm{r,a}}^{-1} & \mathbf{Z}_{\mathrm{r,a}}^{-1} \end{pmatrix} \cdot \begin{pmatrix} \boldsymbol{F}_{\mathrm{a}}^{+} \\ \boldsymbol{F}_{\mathrm{a}}^{-} \end{pmatrix} \tag{4.7}$$

where we introduced $\boldsymbol{F}_{\mathrm{a}}^{\pm} = \boldsymbol{F}^{\pm}(\boldsymbol{k}_{\mathrm{t}}, z_1)$, $\boldsymbol{F}_{\mathrm{b}}^{\pm} = \boldsymbol{F}^{\pm}(\boldsymbol{k}_{\mathrm{t}}, z_{N-1})$, and $\mathbf{P} = \mathbf{P}(z_{N-1}, z_1)$ for brevity. The split fields on either side of the structure can be written in terms of the excitation fields $\boldsymbol{F}_{\mathrm{a}}^{+}$ and $\boldsymbol{F}_{\mathrm{b}}^{-}$ and the scattering matrix as

$$\begin{pmatrix} \boldsymbol{F}_{\mathrm{a}}^{+} \\ \boldsymbol{F}_{\mathrm{a}}^{-} \end{pmatrix} = \begin{pmatrix} \mathbf{I}_2 & \mathbf{0} \\ \mathbf{S}_{11} & \mathbf{S}_{12} \end{pmatrix} \cdot \begin{pmatrix} \boldsymbol{F}_{\mathrm{a}}^{+} \\ \boldsymbol{F}_{\mathrm{b}}^{-} \end{pmatrix} = \left[\begin{pmatrix} \mathbf{I}_2 & \mathbf{0} \\ \mathbf{0} & \mathbf{0} \end{pmatrix} + \begin{pmatrix} \mathbf{0} & \mathbf{0} \\ \mathbf{I}_2 & \mathbf{0} \end{pmatrix} \cdot \begin{pmatrix} \mathbf{S}_{11} & \mathbf{S}_{12} \\ \mathbf{S}_{21} & \mathbf{S}_{22} \end{pmatrix} \right] \cdot \begin{pmatrix} \boldsymbol{F}_{\mathrm{a}}^{+} \\ \boldsymbol{F}_{\mathrm{b}}^{-} \end{pmatrix} \tag{4.8}$$

$$\begin{pmatrix} \boldsymbol{F}_{\mathrm{b}}^{+} \\ \boldsymbol{F}_{\mathrm{b}}^{-} \end{pmatrix} = \begin{pmatrix} \mathbf{S}_{21} & \mathbf{S}_{22} \\ \mathbf{0} & \mathbf{I}_2 \end{pmatrix} \cdot \begin{pmatrix} \boldsymbol{F}_{\mathrm{a}}^{+} \\ \boldsymbol{F}_{\mathrm{b}}^{-} \end{pmatrix} = \left[\begin{pmatrix} \mathbf{0} & \mathbf{0} \\ \mathbf{0} & \mathbf{I}_2 \end{pmatrix} + \begin{pmatrix} \mathbf{0} & \mathbf{I}_2 \\ \mathbf{0} & \mathbf{0} \end{pmatrix} \cdot \begin{pmatrix} \mathbf{S}_{11} & \mathbf{S}_{12} \\ \mathbf{S}_{21} & \mathbf{S}_{22} \end{pmatrix} \right] \cdot \begin{pmatrix} \boldsymbol{F}_{\mathrm{a}}^{+} \\ \boldsymbol{F}_{\mathrm{b}}^{-} \end{pmatrix} \tag{4.9}$$

With arbitrary excitations $\boldsymbol{F}_{\mathrm{a}}^{+}$ and $\boldsymbol{F}_{\mathrm{b}}^{-}$, we find that insertion of these expressions in (4.7) yields a matrix equation

$$\left[\begin{pmatrix}\mathbf{0} & \mathbf{I}_2\\ \mathbf{0} & -\mathbf{Z}_{\mathrm{r,b}}^{-1}\end{pmatrix}-\mathbf{P}\cdot\begin{pmatrix}\mathbf{I}_2 & \mathbf{0}\\ \mathbf{Z}_{\mathrm{r,a}}^{-1} & \mathbf{0}\end{pmatrix}\right]\cdot\begin{pmatrix}\mathbf{S}_{11} & \mathbf{S}_{12}\\ \mathbf{S}_{21} & \mathbf{S}_{22}\end{pmatrix}=\mathbf{P}\cdot\begin{pmatrix}\mathbf{I}_2 & \mathbf{0}\\ -\mathbf{Z}_{\mathrm{r,a}}^{-1} & \mathbf{0}\end{pmatrix}-\begin{pmatrix}\mathbf{0} & \mathbf{I}_2\\ \mathbf{0} & \mathbf{Z}_{\mathrm{r,b}}^{-1}\end{pmatrix} \tag{4.10}$$

From this equation, one could solve directly for the scattering matrix $\mathbf{S}$, but this only leads to the instabilities explored in the previous section. Instead, we use the spectral decomposition (4.5), which yields

$$\begin{aligned}\left[\mathbf{U}^{\dagger}\cdot\begin{pmatrix}\mathbf{0} & \mathbf{I}_2\\ \mathbf{0} & -\mathbf{Z}_{\mathrm{r,b}}^{-1}\end{pmatrix}-\mathbf{D}\cdot\mathbf{U}^{\dagger}\cdot\begin{pmatrix}\mathbf{I}_2 & \mathbf{0}\\ \mathbf{Z}_{\mathrm{r,a}}^{-1} & \mathbf{0}\end{pmatrix}\right]\cdot\begin{pmatrix}\mathbf{S}_{11} & \mathbf{S}_{12}\\ \mathbf{S}_{21} & \mathbf{S}_{22}\end{pmatrix}&\\ =\left[\mathbf{D}\cdot\mathbf{U}^{\dagger}\cdot\begin{pmatrix}\mathbf{I}_2 & \mathbf{0}\\ -\mathbf{Z}_{\mathrm{r,a}}^{-1} & \mathbf{0}\end{pmatrix}-\mathbf{U}^{\dagger}\cdot\begin{pmatrix}\mathbf{0} & \mathbf{I}_2\\ \mathbf{0} & \mathbf{Z}_{\mathrm{r,b}}^{-1}\end{pmatrix}\right]&\end{aligned} \tag{4.11}$$

To make (4.11) stable and avoid propagation factors that are both large and small, identify propagation factors satisfying $|\mathrm{e}^{\mathrm{i}k_0 dn_m}|>1$ (this could correspond to any number of modes, but for the sake of clarity we assume here these are $m=1$ and $m=2$) and divide the equations by these. Note that the eigenvectors $\mathbf{U}^{\dagger}$ and eigenvalues n_m are computed from the eigenproblem for $\mathbf{M}$, and $\mathbf{P}$ is never explicitly computed. The result is

$$\begin{aligned}\left[\mathbf{D}_{-}\cdot\mathbf{U}^{\dagger}\cdot\begin{pmatrix}\mathbf{0} & \mathbf{I}_2\\ \mathbf{0} & -\mathbf{Z}_{\mathrm{r,b}}^{-1}\end{pmatrix}-\mathbf{D}_{+}\cdot\mathbf{U}^{\dagger}\cdot\begin{pmatrix}\mathbf{I}_2 & \mathbf{0}\\ \mathbf{Z}_{\mathrm{r,a}}^{-1} & \mathbf{0}\end{pmatrix}\right]\cdot\begin{pmatrix}\mathbf{S}_{11} & \mathbf{S}_{12}\\ \mathbf{S}_{21} & \mathbf{S}_{22}\end{pmatrix}&\\ =\left[\mathbf{D}_{+}\cdot\mathbf{U}^{\dagger}\cdot\begin{pmatrix}\mathbf{I}_2 & \mathbf{0}\\ -\mathbf{Z}_{\mathrm{r,a}}^{-1} & \mathbf{0}\end{pmatrix}-\mathbf{D}_{-}\cdot\mathbf{U}^{\dagger}\cdot\begin{pmatrix}\mathbf{0} & \mathbf{I}_2\\ \mathbf{0} & \mathbf{Z}_{\mathrm{r,b}}^{-1}\end{pmatrix}\right]&\end{aligned} \tag{4.12}$$

where

$$\mathbf{D}_{-}=\begin{pmatrix}\mathrm{e}^{-\mathrm{i}k_0 dn_1} & 0 & 0 & 0\\ 0 & \mathrm{e}^{-\mathrm{i}k_0 dn_2} & 0 & 0\\ 0 & 0 & 1 & 0\\ 0 & 0 & 0 & 1\end{pmatrix}\quad\text{and}\quad\mathbf{D}_{+}=\begin{pmatrix}1 & 0 & 0 & 0\\ 0 & 1 & 0 & 0\\ 0 & 0 & \mathrm{e}^{\mathrm{i}k_0 dn_3} & 0\\ 0 & 0 & 0 & \mathrm{e}^{\mathrm{i}k_0 dn_4}\end{pmatrix} \tag{4.13}$$

Thus, by dividing by the potentially large exponential functions, all coefficients have finite amplitude leading to a well-conditioned form [12]

$$\begin{aligned}\mathbf{S}=\begin{pmatrix}\mathbf{S}_{11} & \mathbf{S}_{12}\\ \mathbf{S}_{21} & \mathbf{S}_{22}\end{pmatrix}=\left[\mathbf{D}_{-}\cdot\mathbf{U}^{\dagger}\cdot\begin{pmatrix}\mathbf{0} & \mathbf{I}_2\\ \mathbf{0} & -\mathbf{Z}_{\mathrm{r,b}}^{-1}\end{pmatrix}-\mathbf{D}_{+}\cdot\mathbf{U}^{\dagger}\cdot\begin{pmatrix}\mathbf{I}_2 & \mathbf{0}\\ \mathbf{Z}_{\mathrm{r,a}}^{-1} & \mathbf{0}\end{pmatrix}\right]^{-1}&\\ \cdot\left[\mathbf{D}_{+}\cdot\mathbf{U}^{\dagger}\cdot\begin{pmatrix}\mathbf{I}_2 & \mathbf{0}\\ -\mathbf{Z}_{\mathrm{r,a}}^{-1} & \mathbf{0}\end{pmatrix}-\mathbf{D}_{-}\cdot\mathbf{U}^{\dagger}\cdot\begin{pmatrix}\mathbf{0} & \mathbf{I}_2\\ \mathbf{0} & \mathbf{Z}_{\mathrm{r,b}}^{-1}\end{pmatrix}\right]&\end{aligned} \tag{4.14}$$

A special case of interest, is when the thickness of the slab is zero *i.e.*, $d=0$ ($\mathbf{D}_{+}=\mathbf{D}_{-}=\mathbf{I}$), then the above equation becomes

$$\mathbf{S}=\begin{pmatrix}\mathbf{S}_{11} & \mathbf{S}_{12}\\ \mathbf{S}_{21} & \mathbf{S}_{22}\end{pmatrix}=\begin{pmatrix}-\mathbf{I}_2 & \mathbf{I}_2\\ -\mathbf{Z}_{\mathrm{r,a}}^{-1} & -\mathbf{Z}_{\mathrm{r,b}}^{-1}\end{pmatrix}^{-1}\cdot\begin{pmatrix}\mathbf{I}_2 & -\mathbf{I}_2\\ -\mathbf{Z}_{\mathrm{r,a}}^{-1} & -\mathbf{Z}_{\mathrm{r,b}}^{-1}\end{pmatrix} \tag{4.15}$$

which is considered as an interface scattering matrix that describe layers with zero thickness.

In the case of PEC backing, we use $-\eta_0 \boldsymbol{J}_{\mathrm{S}} = \mathbf{g}^+ \cdot \boldsymbol{F}_{\mathrm{a}}^+$ and $\boldsymbol{F}_{\mathrm{a}}^- = \mathbf{r}^+ \cdot \boldsymbol{F}_{\mathrm{a}}^+$ to rewrite (2.18) as a matrix equation

$$\begin{pmatrix} \mathbf{0} \\ \mathbf{g}^+ \end{pmatrix} = \mathbf{P} \cdot \begin{pmatrix} \mathbf{I}_2 & \mathbf{I}_2 \\ -\mathbf{Z}_{\mathrm{r,a}}^{-1} & \mathbf{Z}_{\mathrm{r,a}}^{-1} \end{pmatrix} \cdot \begin{pmatrix} \mathbf{I}_2 \\ \mathbf{r}^+ \end{pmatrix} \tag{4.16}$$

Writing

$$\begin{pmatrix} \mathbf{0} \\ \mathbf{g}^+ \end{pmatrix} = \begin{pmatrix} \mathbf{0} & \mathbf{0} \\ \mathbf{0} & \mathbf{I}_2 \end{pmatrix} \cdot \begin{pmatrix} \mathbf{r}^+ \\ \mathbf{g}^+ \end{pmatrix} \quad \text{and} \quad \begin{pmatrix} \mathbf{I}_2 \\ \mathbf{r}^+ \end{pmatrix} = \begin{pmatrix} \mathbf{I}_2 \\ \mathbf{0} \end{pmatrix} + \begin{pmatrix} \mathbf{0} & \mathbf{0} \\ \mathbf{I}_2 & \mathbf{0} \end{pmatrix} \cdot \begin{pmatrix} \mathbf{r}^+ \\ \mathbf{g}^+ \end{pmatrix} \tag{4.17}$$

and applying the same spectral decomposition and dividing by exponential factors larger than unity, we find

$$\begin{pmatrix} \mathbf{r}^+ \\ \mathbf{g}^+ \end{pmatrix} = \left[\mathbf{D}_- \cdot \mathbf{U}^\dagger \cdot \begin{pmatrix} \mathbf{0} & \mathbf{0} \\ \mathbf{0} & \mathbf{I}_2 \end{pmatrix} - \mathbf{D}_+ \cdot \mathbf{U}^\dagger \cdot \begin{pmatrix} \mathbf{I}_2 & \mathbf{0} \\ \mathbf{Z}_{\mathrm{r,a}}^{-1} & \mathbf{0} \end{pmatrix} \right]^{-1} \cdot \mathbf{D}_+ \cdot \mathbf{U}^\dagger \cdot \begin{pmatrix} \mathbf{I}_2 \\ -\mathbf{Z}_{\mathrm{r,a}}^{-1} \end{pmatrix} \tag{4.18}$$

From these equations the reflection dyadic $\mathbf{r}^+$ and conductance dyadic $\mathbf{g}^+$ can be computed in a numerically stable manner.

5 Composition of slabs and the star product

The technique in Section 4.3 enables the computation of scattering matrices in a stable and numerically robust manner in all layers even where evanescent wave fields are present. The composition of a given stack of materials in terms of given scattering matrices is then made by use of the Redheffer star product [27]. This is in contrast to the transfer matrix formulation where the composition of slabs is made by ordinary matrix multiplication. The star product is a cascading technique by which several substructures that have been analyzed individually can be connected together [31].

The star product combines the individual scattering matrices $\mathbf{S}^{(1)}$ and $\mathbf{S}^{(2)}$ of two material slabs, both assumed embedded in a reference background material with relative wave impedance $\mathbf{Z}_{\mathrm{r},0}$, by

$$\mathbf{S} = \mathbf{S}^{(1)} \bigstar \mathbf{S}^{(2)} \tag{5.1}$$

where the combined scattering matrix $\mathbf{S}$ is defined by

$$\mathbf{S} = \begin{pmatrix} \mathbf{S}_{11} & \mathbf{S}_{12} \\ \mathbf{S}_{21} & \mathbf{S}_{22} \end{pmatrix} \tag{5.2}$$

whit the block dyadics

$$\begin{cases} \mathbf{S}_{11} = \mathbf{S}_{11}^{(1)} + \mathbf{S}_{12}^{(1)} \cdot \left[\mathbf{I}_2 - \mathbf{S}_{11}^{(2)} \cdot \mathbf{S}_{22}^{(1)} \right]^{-1} \cdot \mathbf{S}_{11}^{(2)} \cdot \mathbf{S}_{21}^{(1)} \\ \mathbf{S}_{12} = \mathbf{S}_{12}^{(1)} \cdot \left[\mathbf{I}_2 - \mathbf{S}_{11}^{(2)} \cdot \mathbf{S}_{22}^{(1)} \right]^{-1} \cdot \mathbf{S}_{12}^{(2)} \\ \mathbf{S}_{21} = \mathbf{S}_{21}^{(2)} \cdot \left[\mathbf{I}_2 - \mathbf{S}_{22}^{(1)} \cdot \mathbf{S}_{11}^{(2)} \right]^{-1} \cdot \mathbf{S}_{21}^{(1)} \\ \mathbf{S}_{22} = \mathbf{S}_{22}^{(2)} + \mathbf{S}_{21}^{(2)} \cdot \left[\mathbf{I}_2 - \mathbf{S}_{22}^{(1)} \cdot \mathbf{S}_{11}^{(2)} \right]^{-1} \cdot \mathbf{S}_{22}^{(1)} \cdot \mathbf{S}_{12}^{(2)} \end{cases} \tag{5.3}$$

assuming that $\left[\mathbf{I}_2 - \mathbf{S}_{11}^{(2)} \cdot \mathbf{S}_{22}^{(1)}\right]$ and $\left[\mathbf{I}_2 - \mathbf{S}_{22}^{(1)} \cdot \mathbf{S}_{11}^{(2)}\right]$ are invertible, see *e.g.*, [27, 31]. The product has the property of being dissipative which is fundamental in order to keep the scattering matrix formulation numerical stable when composition of slabs is considered, see Appendix E for details.

Compositions consisting of more than two slabs is performed by recursively evaluating the star products

$$\mathbf{S}^{(\mathrm{tot})} = \mathbf{S}^{(1)} \star \mathbf{S}^{(2)} \star \ldots \star \mathbf{S}^{(N)} \tag{5.4}$$

where N denotes the number of slabs. Equation (5.4) assumes the star product being associative.

Having computed a scattering matrix $\mathbf{S}^{(\mathrm{tot})}$ for a material stack with respect to a reference background material impedance $\mathbf{Z}_{\mathrm{r},0}$, we get the final and so called global scattering matrix with respect to the embedding materials a and b as

$$\mathbf{S}^{(\mathrm{global})} = \mathbf{S}^{(\mathrm{a})} \star \mathbf{S}^{(\mathrm{tot})} \star \mathbf{S}^{(\mathrm{b})} \tag{5.5}$$

where $\mathbf{S}^{(\mathrm{a})}$ is the interface scattering matrix with material a on the left and reference material 0 on the right, whereas $\mathbf{S}^{(\mathrm{b})}$ is the interface scattering matrix with reference material 0 on the left and material b on the right. The additional scattering matrices, see (4.15), are made to describe layers with zero thickness, in order to keep the phase of the total scattering matrix correct [31].

6 Numerical examples

The reformulated propagator formulation according to Section 4, is verified in this section, The examples in Section 3.2 have been recomputed by use of the stabilized formulation of this paper, and the results are presented in Figure 12 through 17.

As shown in Figure 12, are the strong oscillations and above-unity results associated with attenuated fields due to absorption in lossy layers with high thickness/wavelength ratio eliminated by use of the stabilized formulation. Similarly, is it seen in Figure 13 that the new scheme avoids numerical instabilities in the example of tunneling, where strongly attenuated evanescent fields are present.

The exponentially decreasing and increasing wave propagation factors that are present in the examples of the non-magnetic lossless gyrotropic slab, are handled appropriately by the stabilized propagator formulation even for high thickness/wavelength ratios as seen in Figure 14 for the case of a slab enclosed by air and Figure 15, in case of a PEC backed slab.

Figure 16 furthermore, illustrates that the new formulation can treat more complicated structures having strong dispersion in certain frequency bands. Finally, Figure 17 shows that the new scheme is numerical stable even around the center frequency in the stop band of the earlier considered bandgap structure.

The presented examples illustrate that the reformulation of the propagator method in of Section 4, yields stable numerical results in all considered cases of the present paper. However, there is an added numerical cost in the stabilized algorithm from the computation of an eigenvalue problem for the 4×4 matrix $\mathbf{M}$. In most cases, this cost is negligible.

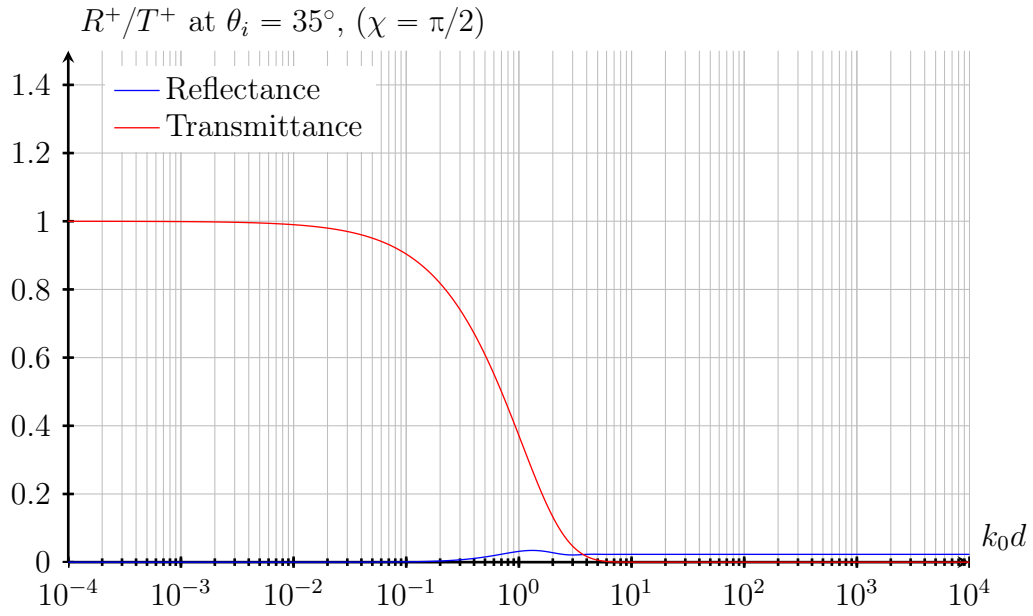

Figure 12: The reflectance and transmittance by use of the stabilized propagator formulation *cf.* Figure 2 in in Section 3.2.3.

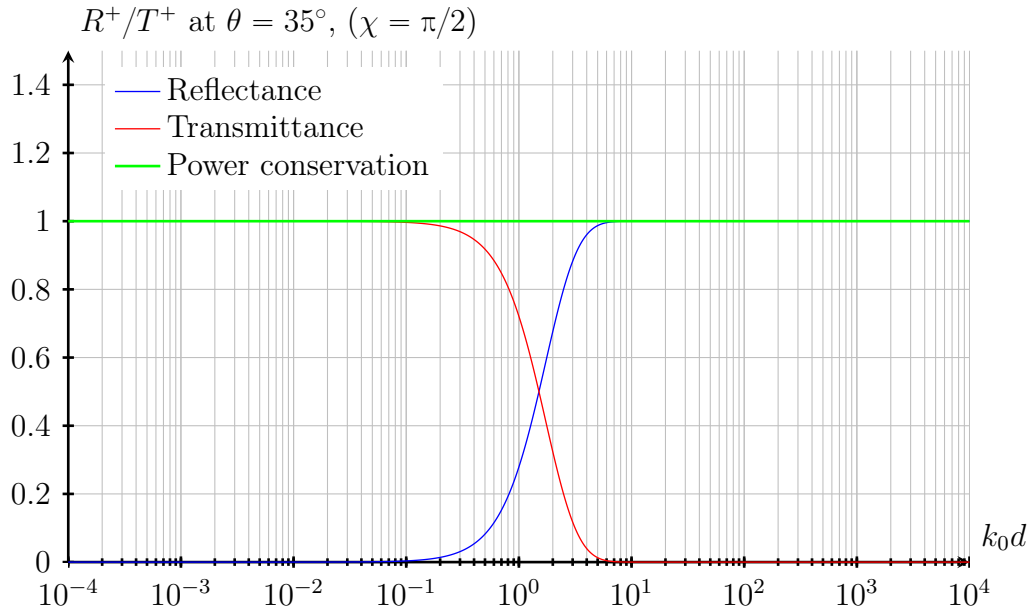

Figure 13: The reflectance and transmittance by use of the stabilized propagator formulation *cf.* Figure 3 in Section 3.2.4.

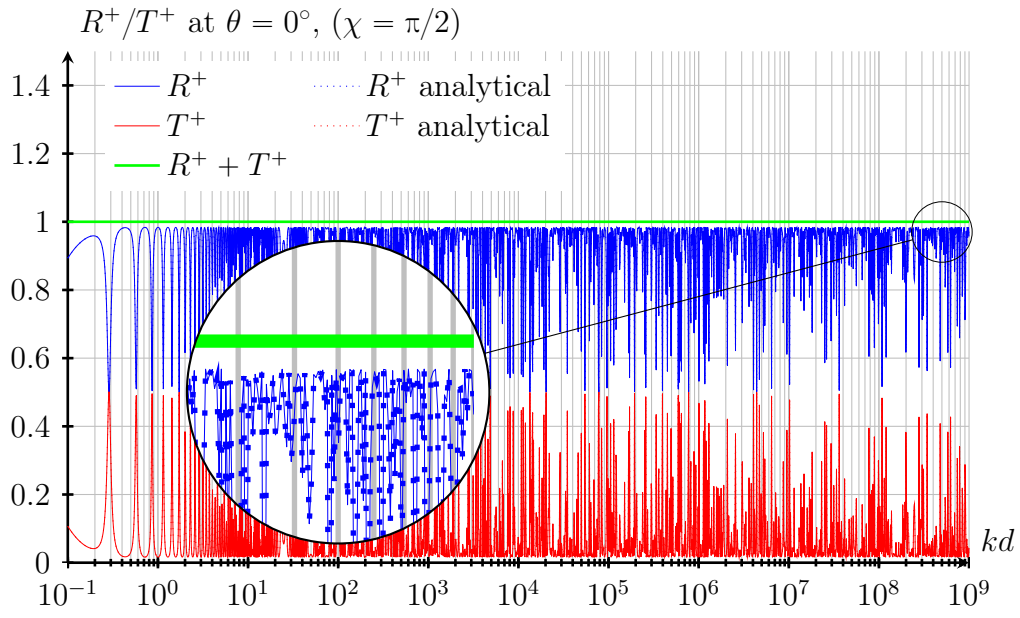

Figure 14: The reflectance and transmittance by use of the stabilized propagator formulation *cf.* Figure 4 in Section 3.2.5.

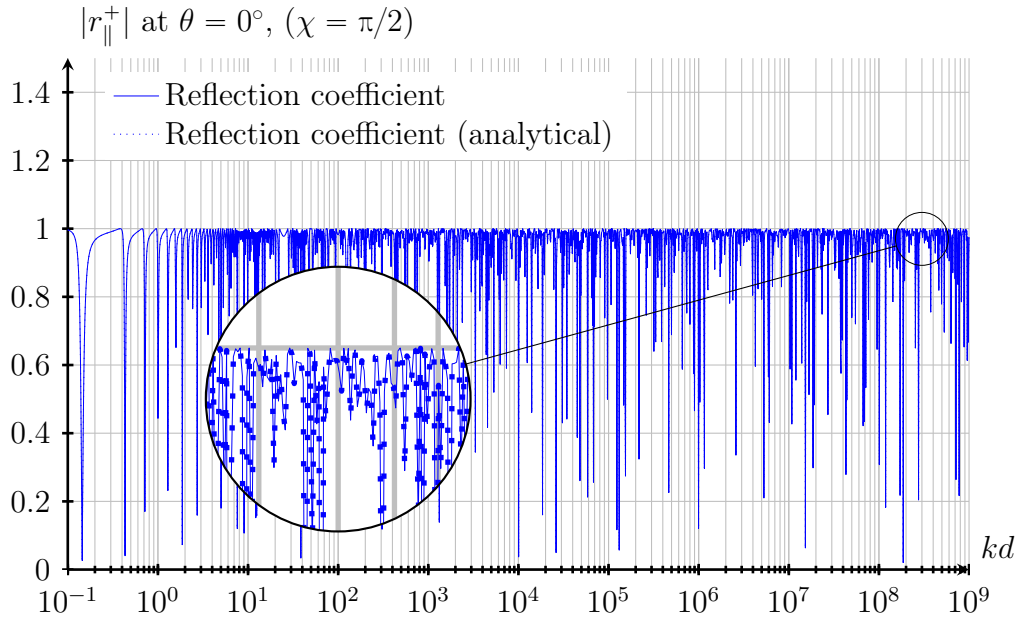

Figure 15: The co-polarized reflection coefficient by use of the stabilized propagator formulation *cf.* Figure 5 in Section 3.2.5.

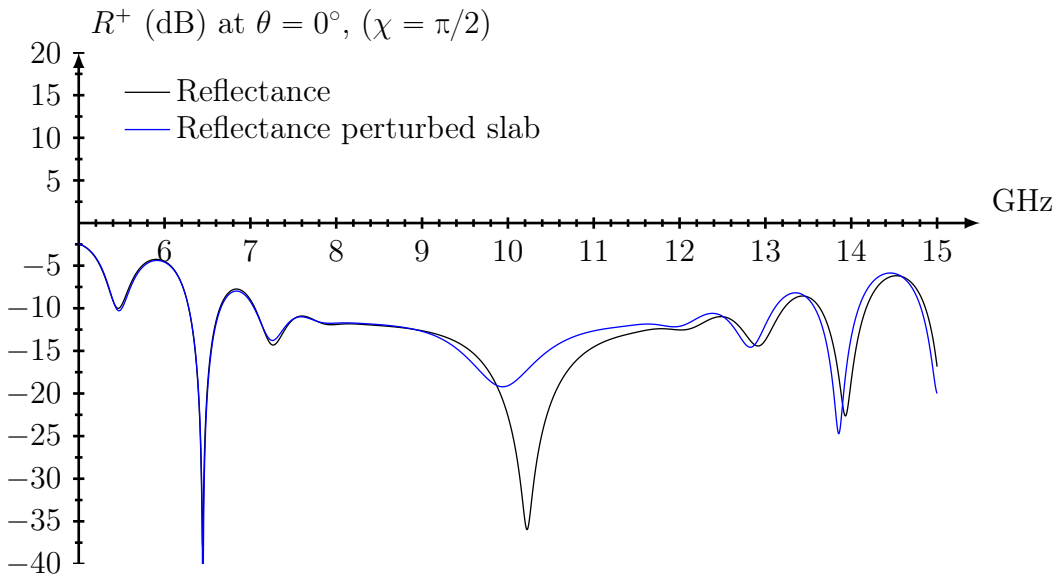

Figure 16: Reflectance by use of the stabilized propagator formulation *cf.* Figure 8 in Section 3.2.6.

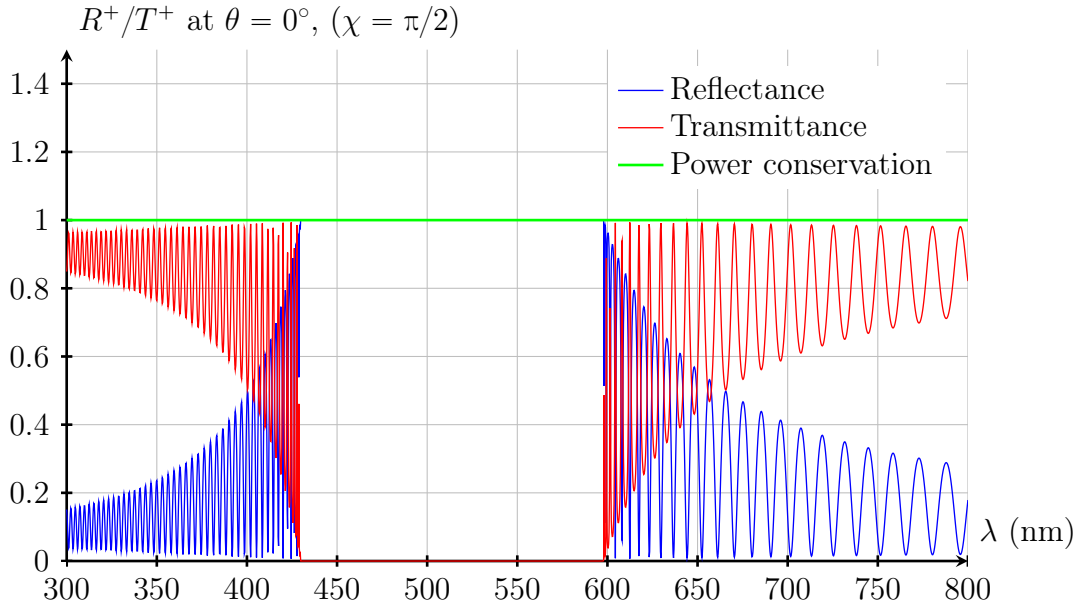

Figure 17: Reflectance and transmittance by use of the stabilized propagator formulation *cf.* Figure 9 in Section 3.2.7.

7 Conclusions

This paper has presented a stabilized scheme that solves the wave propagation problem in a general linear, bianisotropic, stratified media. The method utilizes the concept of propagators, *i.e.*, the wave propagation operators that map the total tangential electric and magnetic fields from one plane in the slab to another. The new scheme transformed the propagator approach into a scattering matrix form, where spectral decomposition of the propagator enabled separation of the exponentially growing and decaying terms in order to obtain a well-conditioned formulation. It was further outlined how multilayer structures can be treated in a stable manner based on the dissipative property of the Redheffer star product for cascading scattering matrices.

The reflection and the transmission dyadics for a general bianisotropic medium with an isotropic half space on both sides of the slab were presented in a coordinate-independent dyadic notation, as well as the reflection dyadic for a bianisotropic slab with perfect electric conductor backing (PEC).

Several numerical examples have been shown with the purpose of motivating the need for stabilization of the propagator formalism as well as for the illustration of the performance of the stabilized algorithm. All considered numerical examples could be computed in a numerically stable manner by the stabilized propagator formulation.

Acknowledgments

The work reported in this paper was supported by grants from Saab Dynamics AB, Linköping, Sweden, which is gratefully acknowledged. The authors also would like to thank Dr. Christer Larsson from Saab Dynamics AB, for the support and helpful discussions about the content of this paper.

A Lateral Fourier transform of the fields

In a geometry where the medium is laterally homogeneous in the variables x and y, it is natural to decompose the electric and magnetic fields and flux densities in a spectrum of plane waves [2]. The fields are decomposed into a spectrum of plane waves by use of the Fourier transform with respect to the lateral position vector $\boldsymbol{\rho} = \hat{\boldsymbol{x}}x + \hat{\boldsymbol{y}}y$ defined by

$$\boldsymbol{E}(\boldsymbol{k}_{\mathrm{t}}, z) = \iint_{-\infty}^{\infty} \boldsymbol{E}(\boldsymbol{r}) \mathrm{e}^{-\mathrm{i}\boldsymbol{k}_{\mathrm{t}}\cdot\boldsymbol{\rho}} \, \mathrm{d}x \, \mathrm{d}y \tag{A.1}$$

where the tangential wave vector $\boldsymbol{k}_{\mathrm{t}} = \hat{\boldsymbol{x}}k_{\mathrm{x}} + \hat{\boldsymbol{y}}k_{\mathrm{y}}$ is real-valued and fixed but arbitrary. The inverse is

$$\boldsymbol{E}(\boldsymbol{r}) = \frac{1}{4\pi^2} \iint_{-\infty}^{\infty} \boldsymbol{E}(\boldsymbol{k}_{\mathrm{t}}, z) \mathrm{e}^{\mathrm{i}\boldsymbol{k}_{\mathrm{t}}\cdot\boldsymbol{\rho}} \, \mathrm{d}k_{\mathrm{x}} \, \mathrm{d}k_{\mathrm{y}} \tag{A.2}$$

and the argument of the field indicates whether the field itself $\boldsymbol{E}(\boldsymbol{r})$ or its Fourier transform $\boldsymbol{E}(\boldsymbol{k}_{\mathrm{t}}, z)$ with respect to $\boldsymbol{\rho}$ is intended.

B Basic equations

B.1 Maxwell source free equations

The dynamics of the fields in a source free region is modeled by time-harmonic Maxwell equations, where time dependence $\mathrm{e}^{-\mathrm{i}\omega t}$ is assumed throughout the paper, *i.e.*,

$$\begin{cases} \nabla \times \boldsymbol{E}(\boldsymbol{r},\omega) = \mathrm{i}k_0\mathrm{c}_0\boldsymbol{B}(\boldsymbol{r},\omega) \\ \eta_0\nabla \times \boldsymbol{H}(\boldsymbol{r},\omega) = -\mathrm{i}k_0\mathrm{c}_0\eta_0\boldsymbol{D}(\boldsymbol{r},\omega) \end{cases} \tag{B.1}$$

where $\mathrm{c}_0 = 1/\sqrt{\epsilon_0\mu_0}$ is the speed of light in vacuum, $k_0 = \omega/\mathrm{c}_0$ is the vacuum wave number and $\eta_0 = \sqrt{\mu_0/\epsilon_0}$ the intrinsic impedance of vacuum, where ϵ_0 and μ_0 denotes the vacuum permittivity and permeability, respectively. The normalization factor η_0 introduced in Ampere's law makes the field quantities having the same order of magnitude.

B.2 Time harmonic constitutive relations

The Maxwell equations (B.1) are usually combined with the constitutive relations, relating the magnetic flux vector $\boldsymbol{B}(\boldsymbol{r},\omega)$ and displacement field $\boldsymbol{D}(\boldsymbol{r},\omega)$ to the electric and magnetic field $\boldsymbol{E}(\boldsymbol{r},\omega)$ and $\boldsymbol{H}(\boldsymbol{r},\omega)$.

The time harmonic constitutive relations of a general bianisotropic medium [14] is given by

$$\begin{cases} \boldsymbol{D} = \epsilon_0 \left\{ \boldsymbol{\epsilon} \cdot \boldsymbol{E} + \eta_0 \boldsymbol{\xi} \cdot \boldsymbol{H} \right\} \\ \boldsymbol{B} = \dfrac{1}{\mathrm{c}_0} \left\{ \boldsymbol{\zeta} \cdot \boldsymbol{E} + \eta_0 \boldsymbol{\mu} \cdot \boldsymbol{H} \right\} \end{cases} \tag{B.2}$$

The bianisotropic medium is the most general linear complex medium fully described by 36 scalar constitutive parameters or functions *i.e.*, the bianisotropic slabs are not restricted to be homogeneous, which means that the slabs may be functions of depth z and/or angular frequency ω (dispersive media). In the lateral directions, x- and y-directions, it is assumed that the material parameters are constant.

B.3 Decomposition of dyadics

For the purpose of studying wave propagation problems in layered bianisotropic structures by the concept of propagators, it is appropriate to decompose each three-dimensional constitutive dyadic into components parallel and perpendicular to the normal of the planar structure, [9, 30]. In general, each three-dimensional constitutive dyadic is decomposed according to

$$\mathbf{A} = \mathbf{A}_{\perp\perp} + \hat{\boldsymbol{z}}\boldsymbol{A}_{\mathrm{z}} + \boldsymbol{A}_{\perp}\hat{\boldsymbol{z}} + \hat{\boldsymbol{z}}A_{\mathrm{zz}}\hat{\boldsymbol{z}} \tag{B.3}$$

where

$$\begin{cases} \mathbf{A}_{\perp\perp} = \mathbf{I}_2 \cdot \mathbf{A} \cdot \mathbf{I}_2 \\ A_{zz} = \hat{\boldsymbol{z}} \cdot \mathbf{A} \cdot \hat{\boldsymbol{z}} \end{cases} \qquad \begin{cases} \boldsymbol{A}_{z} = \hat{\boldsymbol{z}} \cdot \mathbf{A} \cdot \mathbf{I}_2 \\ \boldsymbol{A}_{\perp} = \mathbf{I}_2 \cdot \mathbf{A} \cdot \hat{\boldsymbol{z}} \end{cases} \tag{B.4}$$

The dyadic $\mathbf{A}_{\perp\perp}$ is a two-dimensional dyadic in the x-y plane and the vectors $\boldsymbol{A}_{z}$ and $\boldsymbol{A}_{\perp}$ are two two-dimensional vectors in this plane. A_{zz} is a scalar. Thus, the four dyadics $\boldsymbol{\epsilon}$, $\boldsymbol{\xi}$, $\boldsymbol{\zeta}$ and $\boldsymbol{\mu}$ in the constitutive relations (B.2) for a general bianisotropic medium can be decomposed in tangential and normal parts according to (B.3) *i.e.*,

$$\begin{cases} \boldsymbol{\epsilon} = \boldsymbol{\epsilon}_{\perp\perp} + \hat{\boldsymbol{z}}\boldsymbol{\epsilon}_{z} + \boldsymbol{\epsilon}_{\perp}\hat{\boldsymbol{z}} + \hat{\boldsymbol{z}}\epsilon_{zz}\hat{\boldsymbol{z}} \\ \boldsymbol{\xi} = \boldsymbol{\xi}_{\perp\perp} + \hat{\boldsymbol{z}}\boldsymbol{\xi}_{z} + \boldsymbol{\xi}_{\perp}\hat{\boldsymbol{z}} + \hat{\boldsymbol{z}}\xi_{zz}\hat{\boldsymbol{z}} \\ \boldsymbol{\zeta} = \boldsymbol{\zeta}_{\perp\perp} + \hat{\boldsymbol{z}}\boldsymbol{\zeta}_{z} + \boldsymbol{\zeta}_{\perp}\hat{\boldsymbol{z}} + \hat{\boldsymbol{z}}\zeta_{zz}\hat{\boldsymbol{z}} \\ \boldsymbol{\mu} = \boldsymbol{\mu}_{\perp\perp} + \hat{\boldsymbol{z}}\boldsymbol{\mu}_{z} + \boldsymbol{\mu}_{\perp}\hat{\boldsymbol{z}} + \hat{\boldsymbol{z}}\mu_{zz}\hat{\boldsymbol{z}} \end{cases} \tag{B.5}$$

Using these decompositions, a structured decomposition of the Maxwell equations in components parallel and perpendicular to the normal of the planar structure.

C The fundamental dyadic

The fundamental dyadic $\mathbf{M}(\boldsymbol{k}_t, z)$ is a 4×4 complex-valued dyadic. In a bianisotropic media modelled by the constitutive relations (B.2) the map $\mathbf{M}(\boldsymbol{k}_t, z)$ is explicitly given by [9]

$$\mathbf{M}(\boldsymbol{k}_t, z) = \begin{pmatrix} \mathbf{M}_{11}(\boldsymbol{k}_t, z) & \mathbf{M}_{12}(\boldsymbol{k}_t, z) \\ \mathbf{M}_{21}(\boldsymbol{k}_t, z) & \mathbf{M}_{22}(\boldsymbol{k}_t, z) \end{pmatrix} \tag{C.1}$$

with the block dyadics

$$\begin{cases} \mathbf{M}_{11}(\boldsymbol{k}_t, z) = -\mathbf{J}\cdot\boldsymbol{\zeta}_{\perp\perp} + a(\dfrac{\boldsymbol{k}_t}{k_0} - \mathbf{J}\cdot\boldsymbol{\zeta}_{\perp})(-\mu_{zz}\boldsymbol{\epsilon}_{z} - \xi_{zz}\mathbf{J}\cdot\dfrac{\boldsymbol{k}_t}{k_0} + \xi_{zz}\boldsymbol{\zeta}_{z}) \\ \qquad\qquad - a(\mathbf{J}\cdot\boldsymbol{\mu}_{\perp})(\zeta_{zz}\boldsymbol{\epsilon}_{z} + \epsilon_{zz}\mathbf{J}\cdot\dfrac{\boldsymbol{k}_t}{k_0} - \epsilon_{zz}\boldsymbol{\zeta}_{z}) \\ \mathbf{M}_{12}(\boldsymbol{k}_t, z) = \mathbf{J}\cdot\boldsymbol{\mu}_{\perp\perp}\cdot\mathbf{J} + a(\dfrac{\boldsymbol{k}_t}{k_0} - \mathbf{J}\cdot\boldsymbol{\zeta}_{\perp})(\mu_{zz}\dfrac{\boldsymbol{k}_t}{k_0} - \mu_{zz}\mathbf{J}\cdot\boldsymbol{\xi}_{z} + \xi_{zz}\mathbf{J}\cdot\boldsymbol{\mu}_{z}) \\ \qquad\qquad - a(\mathbf{J}\cdot\boldsymbol{\mu}_{\perp})(-\zeta_{zz}\dfrac{\boldsymbol{k}_t}{k_0} + \zeta_{zz}\mathbf{J}\cdot\boldsymbol{\xi}_{z} - \epsilon_{zz}\mathbf{J}\cdot\boldsymbol{\mu}_{z}) \\ \mathbf{M}_{21}(\boldsymbol{k}_t, z) = -\boldsymbol{\epsilon}_{\perp\perp} - a\boldsymbol{\epsilon}_{\perp}(-\mu_{zz}\boldsymbol{\epsilon}_{z} - \xi_{zz}\mathbf{J}\cdot\dfrac{\boldsymbol{k}_t}{k_0} + \xi_{zz}\boldsymbol{\zeta}_{z}) \\ \qquad\qquad + a(\mathbf{J}\cdot\dfrac{\boldsymbol{k}_t}{k_0} - \boldsymbol{\xi}_{\perp})(\zeta_{zz}\boldsymbol{\epsilon}_{z} + \epsilon_{zz}\mathbf{J}\cdot\dfrac{\boldsymbol{k}_t}{k_0} - \epsilon_{zz}\boldsymbol{\zeta}_{z}) \\ \mathbf{M}_{22}(\boldsymbol{k}_t, z) = \boldsymbol{\xi}_{\perp\perp}\cdot\mathbf{J} - a\boldsymbol{\epsilon}_{\perp}(\mu_{zz}\dfrac{\boldsymbol{k}_t}{k_0} - \mu_{zz}\mathbf{J}\cdot\boldsymbol{\xi}_{z} + \xi_{zz}\mathbf{J}\cdot\boldsymbol{\mu}_{z}) \\ \qquad\qquad + a(\mathbf{J}\cdot\dfrac{\boldsymbol{k}_t}{k_0} - \boldsymbol{\xi}_{\perp})(-\zeta_{zz}\dfrac{\boldsymbol{k}_t}{k_0} + \zeta_{zz}\mathbf{J}\cdot\boldsymbol{\xi}_{z} - \epsilon_{zz}\mathbf{J}\cdot\boldsymbol{\mu}_{z}) \end{cases} \tag{C.2}$$

where $a^{-1} = \epsilon_{zz}\mu_{zz} - \xi_{zz}\zeta_{zz}$, and $\mathbf{J} = \hat{\boldsymbol{z}} \times \mathbf{I}_2$ represents a rotation of $\pi/2$ around the z-axis, and $\mathbf{I}_2 = \hat{\boldsymbol{e}}_{\parallel}\hat{\boldsymbol{e}}_{\parallel} + \hat{\boldsymbol{e}}_{\perp}\hat{\boldsymbol{e}}_{\perp}$ is the identity dyadic in $\mathbb{R}^2$ for lateral vectors. Notice

that the four dyadics $\boldsymbol{\epsilon}$, $\boldsymbol{\xi}$, $\boldsymbol{\zeta}$ and $\boldsymbol{\mu}$ depend on z for materials that are stratified in the z direction. In homogeneous regions, the map $\mathbf{M}$ is independent of z, and, specifically, in an isotropic region the fundamental dyadic is

$$\mathbf{M}(\boldsymbol{k}_{\mathrm{t}}) = \begin{pmatrix} \mathbf{0} & -\mu\mathbf{I}_2 + \frac{1}{\epsilon k_0^2}\boldsymbol{k}_{\mathrm{t}}\boldsymbol{k}_{\mathrm{t}} \\ -\epsilon\mathbf{I}_2 - \frac{1}{\mu k_0^2}\boldsymbol{k}_{\mathrm{t}} \times (\boldsymbol{k}_{\mathrm{t}} \times \mathbf{I}_2) & \mathbf{0} \end{pmatrix} \tag{C.3}$$

More explicit examples of the fundamental dyadic $\mathbf{M}$ are found in [9, 30], and for an alternative representation, see [34].

D The relative wave impedance operator

The relation between electric and magnetic fields propagating in the $\pm z$-direction in a simple media are related through the relative wave impedance operator $\mathbf{Z}_{\mathrm{r}}$ by

$$\eta_0 \mathbf{J} \cdot \boldsymbol{H}_{\mathrm{t}}(\boldsymbol{k}_{\mathrm{t}}, z) = \mp \mathbf{Z}_{\mathrm{r}}^{-1}(\boldsymbol{k}_{\mathrm{t}}) \cdot \boldsymbol{E}_{\mathrm{t}}(\boldsymbol{k}_{\mathrm{t}}, z)$$

where (the operator $\mathbf{Z}_{\mathrm{r}}^{-1}$ is commonly referred to as the relative wave admittance operator $\mathbf{Y}_{\mathrm{r}}$)

$$\mathbf{Z}_{\mathrm{r}}^{-1}(\boldsymbol{k}_{\mathrm{t}}) = \frac{1}{\eta}\left(\frac{k}{k_z}\hat{\boldsymbol{e}}_{\parallel}\hat{\boldsymbol{e}}_{\parallel} + \frac{k_z}{k}\hat{\boldsymbol{e}}_{\perp}\hat{\boldsymbol{e}}_{\perp}\right) \tag{D.1}$$

and

$$\mathbf{Z}_{\mathrm{r}}(\boldsymbol{k}_{\mathrm{t}}) = \eta\left(\frac{k_z}{k}\hat{\boldsymbol{e}}_{\parallel}\hat{\boldsymbol{e}}_{\parallel} + \frac{k}{k_z}\hat{\boldsymbol{e}}_{\perp}\hat{\boldsymbol{e}}_{\perp}\right) \tag{D.2}$$

Here $k = k_0\sqrt{\epsilon\mu}$ is the wavenumber, $k_{\mathrm{z}} = (k^2 - k_{\mathrm{t}}^2)^{1/2}$ is the normal wave number, and $k_{\mathrm{t}} = |\boldsymbol{k}_{\mathrm{t}}| = \sqrt{k_{\mathrm{x}}^2 + k_{\mathrm{y}}^2}$ is the lateral wave number which is a non-negative real number, and $\eta = \sqrt{\mu/\epsilon}$, is the relative wave impedance. Finally, are $\hat{\boldsymbol{e}}_{\parallel} = \boldsymbol{k}_{\mathrm{t}}/k_{\mathrm{t}}$ and $\hat{\boldsymbol{e}}_{\perp} = \hat{\boldsymbol{z}} \times \hat{\boldsymbol{e}}_{\parallel}$, othogonal basis vectors corresponding to the TM and TE polarizations, respectively. The branch of the square root for $k_z = (k^2 - k_{\mathrm{t}}^2)^{1/2}$ is chosen so that $\mathrm{Im}(k_z) \geqslant 0$ for $\mathrm{Im}(k) \geqslant 0$ (for time convention $\mathrm{e}^{\mathrm{i}\omega t}$, simply replace $\mathrm{i} \to -\mathrm{i}$, and choose branch for k_z as $\mathrm{Im}(k_z) \leqslant 0$ for $\mathrm{Im}(k) \leqslant 0$). For $k_{\mathrm{t}} = 0$ *i.e.*, at normal incidence, we have $\mathbf{Z}_{\mathrm{r}}^{-1} = \mathbf{I}/\eta$ and $\mathbf{Z}_{\mathrm{r}} = \eta\mathbf{I}$.

E Dissipation property star product

The scattering matrix $\mathbf{S}$ for a given slab can be written in terms of the reflection and transmission dyadics $\mathbf{r}^{\pm}$ and $\mathbf{t}^{\pm}$, respectively *i.e.*,

$$\mathbf{S}^{(i)} = \begin{pmatrix} \mathbf{S}_{11}^{(i)} & \mathbf{S}_{12}^{(i)} \\ \mathbf{S}_{21}^{(i)} & \mathbf{S}_{22}^{(i)} \end{pmatrix} = \begin{pmatrix} \mathbf{r}^{+} & \mathbf{t}^{-} \\ \mathbf{t}^{+} & \mathbf{r}^{-} \end{pmatrix} \tag{E.1}$$

A passive structure is characterized by the property $\|\mathbf{S}\| \leqslant 1$, where $\|\cdot\|$ denotes the operator norm [27, p. 21]. This can be written as inequalities for the reflection and transmission dyadics as

$$|\mathbf{r}^{+}|^2 + |\mathbf{t}^{+}|^2 \leqslant 1 \quad \text{and} \quad |\mathbf{r}^{-}|^2 + |\mathbf{t}^{-}|^2 \leqslant 1 \tag{E.2}$$

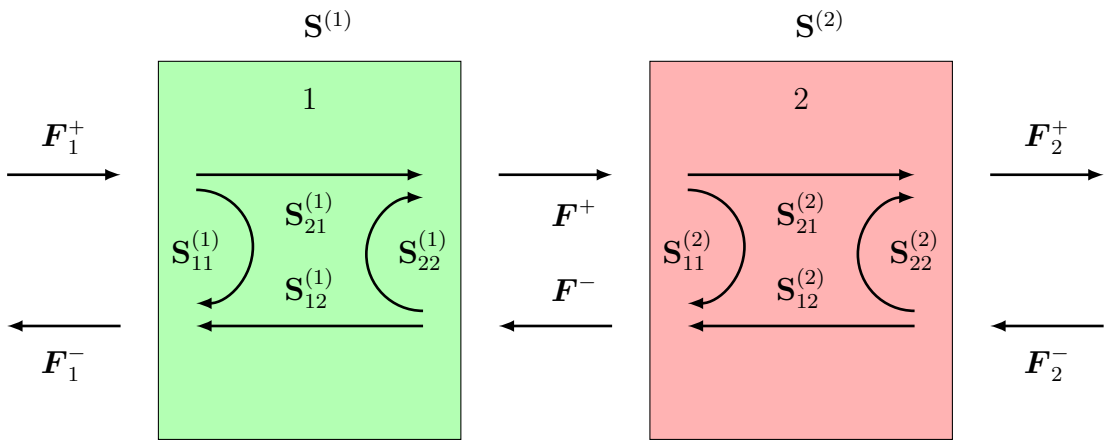

Figure 18: Composition of scattering matrices.

with equality for lossless media. Details on the characterization of passive and lossless media can be found in [9, pp. 57–65].

Consider two scattering matrices $\mathbf{S}^{(1)}$ and $\mathbf{S}^{(2)}$ defined by

$$\begin{pmatrix} \boldsymbol{F}_1^- \\ \boldsymbol{F}^+ \end{pmatrix} = \mathbf{S}^{(1)} \cdot \begin{pmatrix} \boldsymbol{F}_1^+ \\ \boldsymbol{F}^- \end{pmatrix} \quad \text{and} \quad \begin{pmatrix} \boldsymbol{F}^- \\ \boldsymbol{F}_2^+ \end{pmatrix} = \mathbf{S}^{(2)} \cdot \begin{pmatrix} \boldsymbol{F}^+ \\ \boldsymbol{F}_2^- \end{pmatrix} \tag{E.3}$$

and illustrated in Figure 18. If both matrices satisfy $\|\mathbf{S}^{(1,2)}\| \leqslant 1$, we have the dissipation relations

$$|\boldsymbol{F}_1^-|^2 + |\boldsymbol{F}^+|^2 \leqslant |\boldsymbol{F}_1^+|^2 + |\boldsymbol{F}^-|^2 \quad \text{and} \quad |\boldsymbol{F}^-|^2 + |\boldsymbol{F}_2^+|^2 \leqslant |\boldsymbol{F}^+|^2 + |\boldsymbol{F}_2^-|^2 \tag{E.4}$$

The composition of scattering matrices in terms of the star product

$$\begin{pmatrix} \boldsymbol{F}_1^- \\ \boldsymbol{F}_2^+ \end{pmatrix} = \mathbf{S}^{(1)} \bigstar \mathbf{S}^{(2)} \cdot \begin{pmatrix} \boldsymbol{F}_1^+ \\ \boldsymbol{F}_2^- \end{pmatrix} \tag{E.5}$$

preserves the dissipation property *i.e.*,

$$|\boldsymbol{F}_1^-|^2 + |\boldsymbol{F}_2^+|^2 \leqslant |\boldsymbol{F}_1^+|^2 + |\boldsymbol{F}_2^-|^2 \tag{E.6}$$

which is easily found by adding the inequalities above. This result can be extended to any number of slabs, see [27, pp. 22–24].

References

[1] A. Berkhout and A. F. Koenderink. “A simple transfer-matrix model for metasurface multilayer systems”. *Nanophotonics* 9 (12) (2020): pp. 3985–4007.

[2] P. C. Clemmow. “The Plane Wave Spectrum Representation of Electromagnetic Fields”. Pergamon, 1966.

[3] J. Digani, P. W. Hon, and A. R. Davoyan. "Framework for expediting discovery of optimal solutions with blackbox algorithms in non-topology photonic inverse design". *ACS Photonics* 9 (2) (2022): pp. 432–442.

[4] N. Hale, I. Simonsen, C. Brüne, and M. Kildemo. "Use of 4× 4 transfer matrix method in the study of surface magnon polaritons via simulated attenuated total reflection measurements on the antiferromagnetic semiconductor mnf 2". *Physical Review B* 105 (10) (2022): p. 104421.

[5] W. Ji, T. Cai, Z. Xi, and P. Urbach. "Highly efficient and broadband achromatic transmission metasurface to refract and focus in microwave region". *Laser & Photonics Reviews* 16 (1) (2022): p. 2100333.

[6] D. Y. K. Ko and J. Sambles. "Scattering matrix method for propagation of radiation in stratified media: attenuated total reflection studies of liquid crystals". *JOSA A* 5 (11) (1988): pp. 1863–1866.

[7] C. Kohlberger and A. Stelzer. "Multi-modal scattering and propagation through several close periodic grids". *IEEE Transactions on Antennas and Propagation* (2022).

[8] G. Kristensson, S. Poulsen, and S. Rikte. "Propagators and scattering of electromagnetic waves in planar bianisotropic slabs — an application to frequency selective structures". *Progress in Electromagnetics Research* 48 (2004): pp. 1–25.

[9] G. Kristensson. "Scattering of Electromagnetic Waves by Obstacles". Mario Boella Series on Electromagnetism in Information and Communication. SciTech Publishing, 2016.

[10] N. Kumar and J. Saraf. "Tunable reflectance characteristics of magnetized cold plasma based one-dimensional defective photonic crystal". *Optik* 252 (2022): p. 168577.

[11] B. Li and Z. Shen. "Wideband 3d frequency selective rasorber". *IEEE Transactions on Antennas and Propagation* 62 (12) (2014): pp. 6536–6541.

[12] L. Li. "Formulation and comparison of two recursive matrix algorithms for modeling layered diffraction gratings". *JOSA A* 13 (5) (1996): pp. 1024–1035.

[13] Z.-Y. Li and L.-L. Lin. "Photonic band structures solved by a plane-wave-based transfer-matrix method". *Physical Review E* 67 (4) (2003): p. 046607.

[14] I. V. Lindell, A. H. Sihvola, S. A. Tretyakov, and A. J. Viitanen. "Electromagnetic Waves in Chiral and Bi-isotropic Media". Artech House, 1994.

[15] J. M. Luque-Raigon, J. Halme, H. Miguez, and G. Lozano. "Symmetry analysis of the numerical instabilities in the transfer matrix method". *Journal of Optics* 15 (12) (2013): p. 125719.

[16] J.-J. Marigo and A. Maurel. "Second order homogenization of subwavelength stratified media including finite size effect". *SIAM Journal on Applied Mathematics* 77 (2) (2017): pp. 721–743.

[17] C. Menzel, J. Sperrhake, and T. Pertsch. "Efficient treatment of stacked metasurfaces for optimizing and enhancing the range of accessible optical functionalities". *Physical Review A* 93 (6) (2016): p. 063832.

[18] K. A. Michalski. "Modal transmission line theory of plane wave excited layered media with multiple conductive anisotropic sheets at the interfaces". *Journal of Quantitative Spectroscopy and Radiative Transfer* 226 (2019): pp. 19–28.

[19] J. Ning and E. L. Tan. "Hybrid matrix method for stable analysis of electromagnetic waves in stratified bianisotropic media". *IEEE microwave and wireless components letters* 18 (10) (2008): pp. 653–655.

[20] M Norgren. "Optimal design using stratified bianisotropic media: application to anti-reflection coatings". *Journal of electromagnetic waves and applications* 12 (7) (1998): pp. 939–959.

[21] M. Norgren. "Wave-Splitting Approaches to Direct and Inverse Frequency-Domain Scattering of Electromagnetic Waves from Stratified Bianisotropic Materials". PhD thesis. Royal Institute of Technology, 1996.

[22] S. Orfanidis. "Electromagnetic Waves and Antennas". Sophocles J. Orfanidis, 2016.

[23] A. Ourir, Y. Gao, A. Maurel, and J.-J. Marigo. *Homogenization of thin and thick metamaterials and applications*. 2017.

[24] J. Pendry. "Photonic band structures". *Journal of modern optics* 41 (2) (1994): pp. 209–229.

[25] D. M. Pozar. "Microwave Engineering". John Wiley & Sons, 1998.

[26] A. Ranjbar and A. Grbic. "Analysis and synthesis of cascaded metasurfaces using wave matrices". *Physical Review B* 95 (20) (2017): p. 205114.

[27] R. Redheffer. "On the relation of transmission-line theory on scattering and transfer". *J. Math. Phys.* 41 (1962): pp. 1–41.

[28] J. Riga and R. Seviour. "Electromagnetic analogs of quantum mechanical tunneling". *Journal of Applied Physics* 132 (20) (2022): p. 200901.

[29] S. Rikte, M. Andersson, and G. Kristensson. "Homogenization of woven materials". *Archiv für Elektronik und Übertragungstechnik (AEÜ)* 53 (5) (1999): pp. 261–271.

[30] S. Rikte, G. Kristensson, and M. Andersson. "Propagation in bianisotropic media—reflection and transmission". *IEE Proc. Microwaves, Antennas and Propagation* 148 (1) (2001): pp. 29–36.

[31] R. C. Rumpf. "Improved formulation of scattering matrices for semi-analytical methods that is consistent with convention". *Progress In Electromagnetics Research B* 35 (2011): pp. 241–261.

[32] M. G. Silveirinha and C. A. Fernandes. "Homogenization of metamaterial surfaces and slabs: the crossed wire mesh canonical problem". *IEEE transactions on antennas and propagation* 53 (1) (2005): pp. 59–69.

[33] D. Sjöberg. "Analysis of wave propagation in stratified structures using circuit analogs, with application to electromagnetic absorbers". *Eur. J. Phys.* 29 (2008): pp. 721–734.

[34] D. Sjöberg. "Circuit analogs for wave propagation in stratified structures". In: *Wave Propagation in Materials for Modern Applications*. Ed. by A. Petrin. InTech, 2010, pp. 489–508.

[35] J. Sperrhake, M. Decker, M. Falkner, S. Fasold, T. Kaiser, I. Staude, and T. Pertsch. "Analyzing the polarization response of a chiral metasurface stack by semi-analytic modeling". *Optics Express* 27 (2) (2019): pp. 1236–1248.

[36] H.-Y. D. Yang. "A spectral recursive transformation method for electromagnetic waves in generalized anisotropic layered media". *IEEE Trans. Antennas Propagat.* 45 (3) (1997): pp. 520–526.

[37] Y. Yu, G. Q. Luo, A. A. Omar, X. Liu, W. Yu, Z. C. Hao, and Z. Shen. "3d absorptive frequency-selective reflection and transmission structures with dual absorption bands". *IEEE Access* 6 (2018): pp. 72880–72888.

[38] Z. A. Zaky, A. Panda, P. D. Pukhrambam, and A. H. Aly. "The impact of magnetized cold plasma and its various properties in sensing applications". *Scientific Reports* 12 (1) (2022): pp. 1–12.